

## ABSTRACT

SMITH, RYAN MICHAEL. A Model for Mechanical Circuit Breaker Arc Mitigation via Pressure Modulation of a Liquid Dielectric in a Parallel Arc Chamber. (Under the direction of Dr. Leonard W. White).

This work conceptualizes a new mechanical circuit breaker that disrupts electric arc formation across the breaker contacts, improving breaker durability, and serves as an alternative to gas insulating breakers. The proposed breaker design places a liquid-filled arc chamber in parallel with the main breaker contacts. The liquid in the arc chamber serves as a dielectric medium whose dielectric properties may be externally manipulated by environmental factors such as pressure. As the breaker opens during a fault condition, the breaker design forces the electric arc to transfer to the arc chamber, at which point actuation of a piezoelectric transducer array modulates the pressure of the liquid, temporarily elevating the breakdown voltage in the chamber and extinguishing the electric arc.

This work presents two MATLAB/Simulink models to assess the feasibility of the new breaker concept. The first shows that as the main breaker contacts open, a changing relationship between the conductance of the dielectric medium in the breaker (air) and the conductance of the dielectric medium in the arc chamber (liquid) forces any electric arc that forms to transfer from the main breaker contacts to the arc chamber electrodes. The second model shows that high-pressure shock waves created by a piezoelectric transducer array alter the pressure and density of the liquid dielectric, momentarily raising the breakdown voltage associated with the liquid.

© Copyright 2024 by Ryan Smith  
All Rights Reserved.

A Model for Mechanical Circuit Breaker Arc Mitigation via Pressure Modulation of a Liquid Dielectric in a Parallel Arc Chamber

by  
Ryan Smith

A thesis submitted to the Graduate Faculty of  
North Carolina State University  
in partial fulfillment of the  
requirements for the degree of  
Master of Science

Electrical Engineering

Raleigh, North Carolina

2024

APPROVED BY:

---

Leonard White  
Chair of Advisory Committee

---

Subhashish Bhattacharya

---

Mesut Baran

## DEDICATION

To my wife, **Meghan**, who did everything in her power to support me during my graduate education.

To my children, **Izzy** and **Noah**, who did everything in their power to distract me during my graduate education.

## ACKNOWLEDGMENTS

There are many people that I would like to thank for their support throughout my Master's education. However, there are several people whom I would like to name specifically.

First, I would like to specifically thank Dr. White for his guidance and instruction throughout my Master's education. I am grateful that he, as well as Dr. Baran and Dr. Bhattacharya, were eager to advise an online, remote graduate student in a Master's thesis.

From my time in the Navy, I would also like to thank my former Commanding Officer, Captain Michael Majewski, and former Executive Officer, Commander John Kerr, for facilitating and supporting my graduate education during my time as an instructor at the Penn State Naval Reserve Officers Training Corps.

From my employer, Penn State University, I would also like to thank my supervisor, Joel Anstrom, and my coworkers Rob Richards and Michael Brady for their support in helping me to get across the finish line.

Finally, I would like to thank my wife Meghan for her support throughout my graduate education...and entire marriage for that matter. She ceaselessly worked to raise our two children and keep the family and house in order, usually with a smile and always with love!

## **BIOGRAPHY**

Ryan Smith is a part-time Electrical and Computer Engineering Master's Thesis graduate student at North Carolina State University. Ryan is a native of Newport News, Virginia. He earned his undergraduate degree in Mechanical Engineering from Penn State University in 2016. Upon completion of his undergraduate degree, Ryan served in the United States Navy for seven years as a nuclear submarine officer, which strongly influenced his interest in power systems. Ryan works as a research and development engineer at Penn State University in State College, PA where he develops maritime electrical systems. Ryan continues to serve his country as an officer in the Navy Reserve. Ryan has been married to his wife, Meghan, since 2017. Together, they have two children, Isabel and Noah.

## TABLE OF CONTENTS

<b>LIST OF TABLES .....</b>	<b>vii</b>
<b>LIST OF FIGURES .....</b>	<b>viii</b>
<b>LIST OF ACRONYMS AND SYMBOLS .....</b>	<b>xi</b>
<b>Chapter 1: Introduction .....</b>	<b>1</b>
<b>Chapter 2: Literature Review of Electric Arcs and Arc Extinguishment Techniques.....</b>	<b>4</b>
Review of the Cassie and Mayr Arc Models .....	4
Factors Affecting the Cassie Arc Model.....	4
Historical Basis for High Pressure Arc Extinguishment.....	6
General Principles of Arc Extinguishment .....	6
Potential for Use of Liquid Dielectrics in Arc Extinguishment.....	7
Suggested Mechanisms for Arc Extinguishment by Liquid Dielectrics .....	7
Influence of Existing Lithotripsy Technology .....	8
Methods of Pressure Wave Generation as Applied in Lithotripsy .....	9
<b>Chapter 3: Development of Arc Transfer and Density Modulation Models.....</b>	<b>12</b>
Arc Contact Transfer Model .....	12
Density Modulation Simulation T&D Test System Parameters .....	14
Arc Chamber Model .....	14
Pressure Wave Generation Block .....	16
Pressure-Density Lookup Block .....	18
Density to Breakdown Voltage Block .....	20
<b>Chapter 4: Results and Discussion .....</b>	<b>22</b>
Arc Transfer Simulation Results and Discussion .....	22
Density Modulation Simulation Results and Discussion.....	24
Sensitivity to Different Liquid CO <sub>2</sub> Temperature.....	24
Sensitivity to PZ Voltage .....	27
Sensitivity to System Voltage.....	29
Comparison to SF <sub>6</sub> and Other Gaseous Insulators .....	31
<b>Chapter 5: Additional Considerations .....</b>	<b>34</b>
Dielectric Medium Selection .....	34
Fault Response and PZ Transducer Timing Considerations.....	34

Example Scenario of PZ Timing and Current PZ Technology Limitations .....	36
Possible Methods of Breaker Failure .....	37
<b>Chapter 6: Conclusion.....</b>	<b>39</b>
<b>REFERENCES.....</b>	<b>40</b>
<b>APPENDIX.....</b>	<b>42</b>

## LIST OF TABLES

Table 1.	T&D System Parameters for Breaker Response Simulation .....	14
Table 2.	Summary of Temperature Sensitivity Results .....	25
Table 3.	Summary of Applied PZ Voltage Sensitivity Results.....	28

## LIST OF FIGURES

Figure 1.	Sketch of the physical arrangement of main circuit breaker and its associated parallel arc chamber. ....	1
Figure 2.	Simplified one-line diagram showing the proposed breaker design. ....	2
Figure 3.	Effect of the Cassie time constant on the arc voltage [2]. ....	5
Figure 4.	Effect of the Cassie arc voltage constant on the arc voltage [2]. ....	5
Figure 5.	Increasing arc voltage with increasing electrode gap [2]. ....	6
Figure 6.	Young's experimental results showing increasing breakdown voltage with density in liquid CO <sub>2</sub> [6]. ....	7
Figure 7.	Results from Lesaint and Gournay showing the stopping length of arc streamers in transformer oil at various oil pressures with increasing applied voltage [8]. ....	8
Figure 8.	Resulting pressure shockwave from lithotripter testing by Thomas, et al[11]. Pressure oscillations occur as the pressure shockwave subsides. Positive pressures indicate compression of the liquid. Negative pressures indicate expansion of the liquid. ....	11
Figure 9.	Generic circuit used to model a Cassie arc at 60 Hz. ....	12
Figure 10.	MATLAB/Simulink arc current, arc voltage, and Cassie conductance calculations. ....	13
Figure 11.	MATLAB/Simulink Cassie conductance calculation block. ....	13
Figure 12.	Cassie arc voltage constant determination. ....	14
Figure 13.	MATLAB/Simulink arc chamber spark gap breakdown voltage calculation model. ....	15

Figure 14.	Simulink model of the Pressure Wave Generation Block. ....	16
Figure 15.	Thomas, et al experimental results comparing pressure response when applying maximum differential voltage (red) versus 80% differential voltage (blue) [11].....	17
Figure 16.	Maximum peak pressure versus applied differential voltage. ....	17
Figure 17.	Example of an asymmetrical pressure pulse generated by the PWGB peak pressure calculations. ....	18
Figure 18.	Density of CO <sub>2</sub> versus pressure at 0°C, 15°C, and 30°C. The knee in each curve indicates the transition from gaseous to liquid form with increasing pressure [12].....	19
Figure 19.	Pressure-Density Lookup Block. ....	20
Figure 20.	Density to Breakdown Voltage Block .....	20
Figure 21.	LUT contains a synthesis of Young's experimental results with a linearly extrapolated results above 0.7 g/ml [6]. ....	21
Figure 22.	Arc contact separation versus time. ....	22
Figure 23.	Arc voltage constant versus time. ....	23
Figure 24.	Cassie arc conductance versus time.....	23
Figure 25.	BDV in the arc chamber spark gap, TRV, and source voltage as a function of time with 0°C liquid CO <sub>2</sub> . ....	25
Figure 26.	BDV in the arc chamber spark gap, TRV, and source voltage as a function of time with 15°C liquid CO <sub>2</sub> . ....	26
Figure 27.	BDV in the arc chamber spark gap, TRV, and source voltage as a function of time with 30°C liquid CO <sub>2</sub> . ....	27

Figure 28.	BDV in the arc chamber spark gap, TRV, and source voltage as a function of time when 13.5 kV is applied across the PZ transducer array.....	28
Figure 29.	BDV in the arc chamber spark gap, TRV, and source voltage as a function of time when 15.5 kV is applied across the PZ transducer array.....	29
Figure 30.	BDV in the arc chamber spark gap, TRV, and source voltage as a function of time when 17.5 kV is applied across the PZ transducer array.....	29
Figure 31.	BDV in the arc chamber spark gap, TRV, and source voltage as a function of time when system voltage and apparent power are 7.2 kV and 10 MVA, respectively. ....	30
Figure 32.	BDV in the arc chamber spark gap, TRV, and source voltage as a function of time when system voltage and apparent power are 13.1 kV and 20 MVA, respectively. ....	30
Figure 33.	BDV in the arc chamber spark gap, TRV, and source voltage as a function of time when system voltage and apparent power are 33 kV and 40 MVA, respectively. ....	31
Figure 34.	BDV's for various gases with respect to pressure and gap distance [14]......	32
Figure 35.	Relationship between dielectric strength and gas insulator pressure [14]......	32
Figure 36.	Possible PZ arrangements. A) A PZ array that uses two repeatedly pulsing PZ transducers. B) A PZ array that uses sequentially operating PZ transducer pairs.....	36
Figure 37.	Simulated T&D system prior to fault insertion.....	43
Figure 38.	Simulated T&D system at the time of the fault insertion. ....	44
Figure 39.	Simulated T&D system at the time of fault clearing. ....	46

## LIST OF ACRONYMS AND SYMBOLS

AC	Alternating Current
BDV	Breakdown Voltage
cc	Cubic Centimeter(s)
CO <sub>2</sub>	Carbon Dioxide
DBDVB	Density to Breakdown Voltage Block
DC	Direct Current
g	Gram(s)
Hz	Hertz
kHz	Kilohertz
kV	Kilovolt(s)
LUT	Lookup Table
ml	Milliliter(s)
MPa	Megapascal(s)
MVA	Megavolt-Ampere(s)
PDLB	Pressure-Density Lookup Block
psi	Pound(s) per square inch
PWGB	Pressure Wave Generation Block
PZ	Piezoelectric
SF <sub>6</sub>	Sulfur Hexafluoride
T&D	Transmission and Distribution
TRV	Transient Recovery Voltage
V	Volt(s)
VA	Volt-Ampere(s)
Z	Impedance
μF	Microfarad(s)
Ω	Ohm(s)

## Chapter 1: Introduction

The high voltage Transmission and Distribution (T&D) system requires reliable and durable protective equipment for safe maintenance and operation. One of the cornerstones of alternating current (AC) protective equipment is the Sulfur Hexafluoride ( $\text{SF}_6$ ) breaker, a device that provides protective action in the event of system faults and quenches electrical arcs that may occur during normal system operation. To eliminate or reduce the arc,  $\text{SF}_6$  breakers inject gaseous  $\text{SF}_6$  to quench the arc until the Transient Recovery Voltage (TRV) that may occur subsides after the breaker opens.  $\text{SF}_6$  has the disadvantage of being a stable greenhouse gas, which can enter the atmosphere from leaks and other faults or operations in  $\text{SF}_6$  breaker protection systems [1].

AC systems experience naturally occurring zero-crossings, even during fault conditions. As such, normal AC breakers actuate at the zero-crossing, minimizing the associated TRV. In fast-operating breakers, a current chop may occur prior to a zero-crossing, increasing the possibility of TRV due to the inductive nature of power systems. Because of the current chop and TRV, it is possible that an electric arc may form across the main contacts of the breaker. Electrical arcs pose a risk to equipment and personnel and reduce the equipment's operating life.

The proposed breaker design places a liquid-filled arc-extinguishing chamber (referred to as an "arc chamber" throughout the rest of this paper) in parallel with the main breaker as shown in Figure 1. The arc chamber houses a bank of Piezoelectric (PZ) crystals and a spark gap, as shown in the one-line diagram of Figure 2. A liquid dielectric fills the free space in the arc chamber, submerging the spark gap.

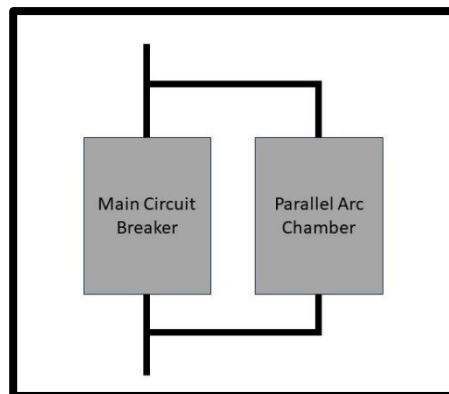


**Figure 1.** Sketch of the physical arrangement of main circuit breaker and its associated parallel arc chamber.

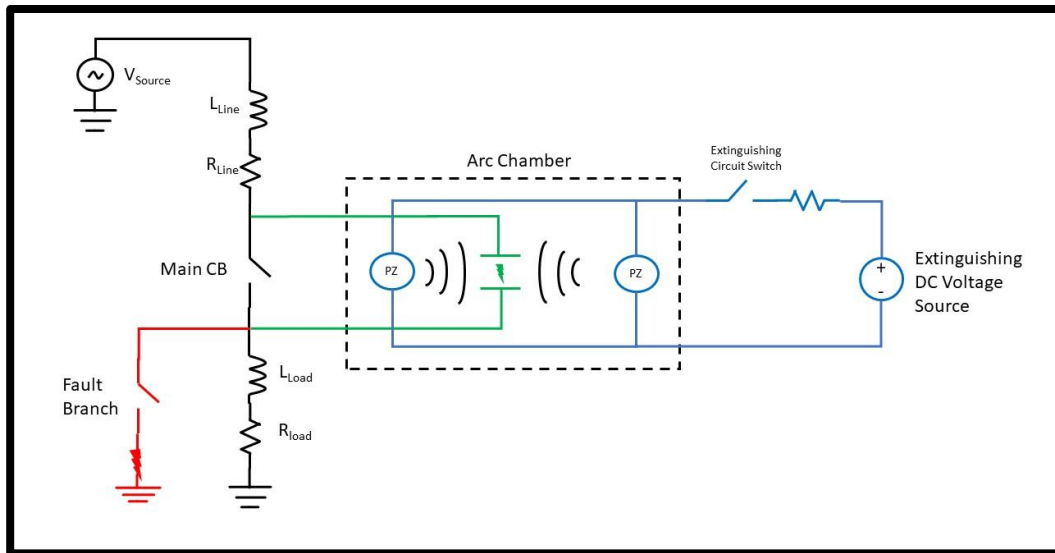


**Figure 2.** Simplified one-line diagram showing the proposed breaker design.

A general summary of the operation of this breaker follows. When the T&D protection system detects a fault, the main breaker operates, and its contacts begin to separate at the current point on the voltage and current waveforms. The inductive nature of the T&D system develops a TRV. As the TRV rises, an electric arc may form across the main breaker contacts. As the breaker opens, the present work suggests that a point occurs in which the conductance between the electrodes in the spark gap of the arc chamber exceeds the conductance between the opening breaker contacts. Therefore, at some point in time, the electric arc transfers from the main breaker contacts to the arc chamber's spark gap. After the arc transfers to the spark gap, PZ transducers trigger a constructively interfering high-pressure shockwave inside the arc chamber. This shockwave momentarily raises the density, and subsequently the breakdown voltage of the liquid dielectric at the shockwave's focal point, above the maximum voltage seen during the TRV. This work further refers to this concept interchangeably as "density modulation" or "pressure modulation." Because the TRV is not sufficient to overcome the artificially elevated breakdown voltage of the high-density liquid dielectric, the arc theoretically extinguishes.

This paper discusses the development and simulation results of two MATLAB/Simulink models used to assess the arc transfer and density modulation in the proposed breaker design. Additionally, this paper provides an in-depth commentary on important assumptions embedded in the models, as well as additional research needed to validate these assumptions. Finally, this paper comments on the feasibility and outlook of this breaker design in practical application.

Given that these models serve as a preliminary investigation or feasibility study regarding this breaker design, these models use empirical data gathered from previously published research, rather than newly collected data, to ground assumptions and provide realistic system responses to inputs.

## Chapter 2: Literature Review of Electric Arcs and Arc Extinguishment Techniques

The following sections summarize the literature review conducted to fully understand the background behind electric arc formation and extinguishment and pressure response of PZ transducers.

### *Review of the Cassie and Mayr Arc Models*

Arc transfer from the main breaker contacts to the arc chamber spark gap is a key operating principle of this novel breaker design. Therefore, a brief review of major arc models provides the necessary background to investigate the ability of an electrical arc to transfer from the gap in one conductor to the gap in another parallel conductor.

The two most general arc models are the Cassie arc model and the Mayr arc model. Equation 1 shows the Cassie arc model where  $g_c$  is the Cassie arc conductivity,  $\tau_c$  is the Cassie arc time constant,  $u$  is the voltage applied to the arc, and  $U_c$  is the Cassie arc voltage constant [2]. Equation 2 shows the Mayr model where  $g_m$  is the Mayr arc conductivity,  $\tau_m$  is the Mayr arc time constant,  $u$  is the voltage applied to the arc,  $i$  is the arc current, and  $P_0$  is the Mayr power dissipation constant [3].

$$(1) \quad \frac{1}{g_c} \frac{dg_c}{dt} = \frac{1}{\tau_c} \left( \frac{u^2}{U_c^2} - 1 \right)$$

$$(2) \quad \frac{d \ln(g_m)}{dt} = \frac{1}{\tau_m} \left( \frac{ui}{P_0} - 1 \right)$$

The Cassie model proves more accurate at high arc currents and assumes a fixed temperature throughout the arc, cooling the arc by forced convection. The Mayr model proves more accurate at low arc currents and assumes that conduction causes arc power losses [2]. Focused on analyzing high-current power system faults and the extinguishment of their associated arcs, the remainder of this paper references the Cassie arc model.

### *Factors Affecting the Cassie Arc Model*

Arc conditions such as electrode material, quenching medium, and gap distance affect the parameters of the Cassie equation. As shown in Figure 3, changing the Cassie time constant has negligible effect on the shape of the arc voltage. However, changing the arc voltage constant

significantly affects the shape of the arc voltage as shown in Figure 4. Consequently, the magnitude of the arc voltage is equal to the arc constant [3].

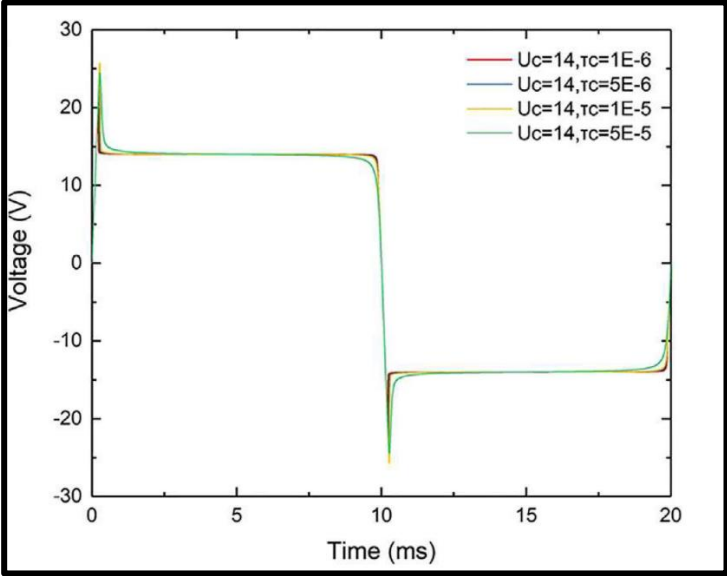


**Figure 3.** Effect of the Cassie time constant on the arc voltage [2].

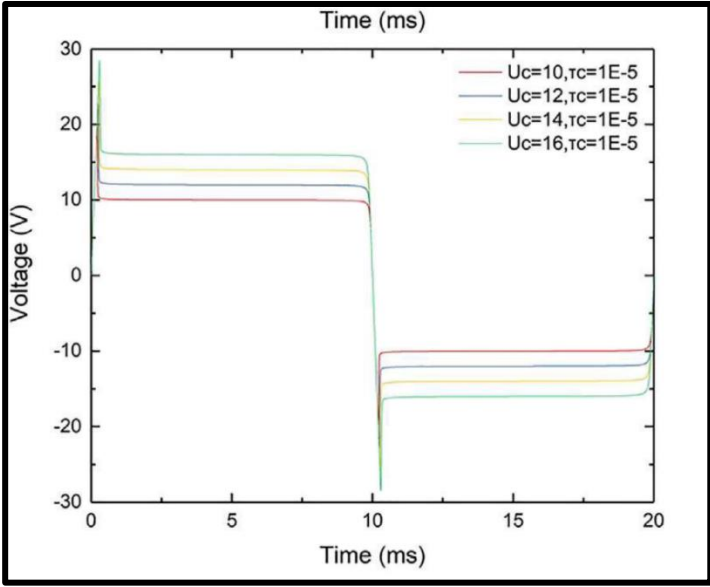


**Figure 4.** Effect of the Cassie arc voltage constant on the arc voltage [2].

Furthermore, as the arc gap becomes larger, the arc voltage becomes larger, as shown in Figure 5. Combining the arc voltage-arc gap relationship with the arc voltage approximation, the conductance between separating breaker contacts could be modeled by allowing the arc voltage constant to increase during simulation.

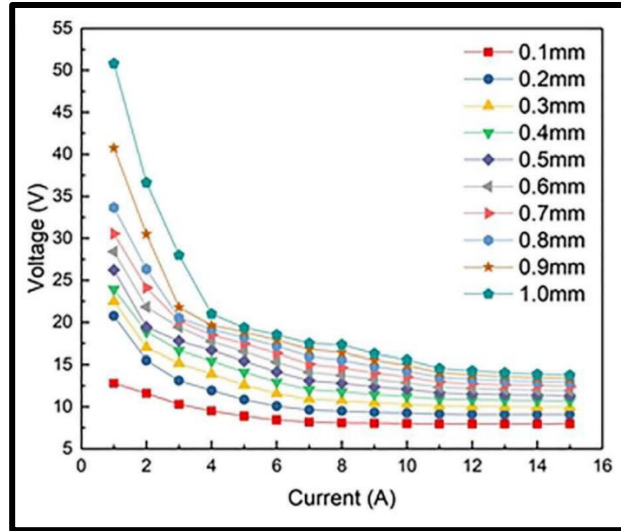


**Figure 5.** Increasing arc voltage with increasing electrode gap [2].

### *Historical Basis for High Pressure Arc Extinguishment*

Previous investigations of using high pressure to extinguish electrical arcs date back to the early 20<sup>th</sup> century. Once such investigation, summarized in US Patent 1127043, proposed a concept for arc extinguishment of line-to-line powerline faults in which a small explosive charge oriented normal to the electric arc displaces the conductor through which the arc travels. The conductor's displacement forces the arc to take a semicircular path between the two electrical contacts, extinguishing the arc [4].

### *General Principles of Arc Extinguishment*

There are several general tenets to AC arc extinguishment as summarized by Alegria [5]. At its core, an AC arc is an ionized gas space. To extinguish the arc, the gas space must be de-ionized by recombining ions to achieve an insulating status. Applied external forces may accelerate the rate of recombination. Examples of external forces include the “gas blast” associated with expulsion fuses [5] or the gas injection associated with SF<sub>6</sub> breakers.

In an AC arc, the current momentarily is zero at the current zero-crossing. At the zero-crossing, the ionization stops, but de-ionization continues, allowing the arcing medium to return to an insulating state. Because some de-ionization has occurred, the voltage applied to continue the arc over the next half cycle must be even larger. Eventually, the required voltage to continue the arc becomes large enough that the arc can no longer re-develop, thus extinguishing the arc [5]. By forcing the arcing medium to remain in an insulating state, the arc extinguishes.

### *Potential for Use of Liquid Dielectrics in Arc Extinguishment*

Research by Young [6] previously investigated the effect of density on breakdown voltage in liquid Carbon Dioxide ( $\text{CO}_2$ ). Young's findings demonstrate that given a fixed spark gap length, the breakdown voltage of liquid  $\text{CO}_2$  increases with increasing liquid density [6]. While  $\text{CO}_2$  is not an ideal fluid for arc extinguishing applications for reasons explained in further detail later, Young's findings, shown in Figure 6, suggest that density modulation may enable a high-pressure shockwave device to raise and maintain the breakdown voltage of a suitable liquid-dielectric to outlast the TRV and extinguish or eliminate an electric arc.

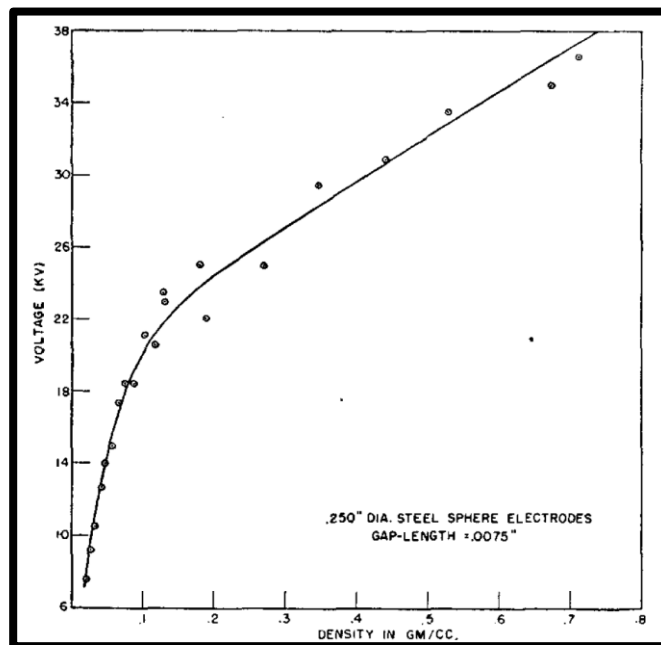


**Figure 6.** Young's experimental results showing increasing breakdown voltage with density in liquid  $\text{CO}_2$  [6].

### *Suggested Mechanisms for Arc Extinguishment by Liquid Dielectrics*

Research by Wedin [7] investigates the significance of streamers in liquid dielectrics as related to dielectric breakdown voltage. Streamers are bubble- and tree-like structures of high conductivity (compared to the surrounding liquid) that develop when a dielectric experiences breakdown. Heat from the electric field causes bubbles to form at or near the electrode. Coalescence of these bubbles forms a streamer. An electron may pass through this streamer and gain sufficient energy to ionize more nearby molecules [7].

Lesaint and Gournay [8] presents findings which discuss the impact of hydrostatic pressure on streamer development in organic liquid dielectrics. This study limited its scope to seven megapascals (MPa), or approximately 1,015 pounds per square inch (psi), and did not consider overvoltage conditions, such as those experienced during a TRV. This research investigated the ability of hydrostatic pressure to reduce the stopping length of the streamer, as measured from the cathode of the arc initiating device. Cited from this study, Figure 7 summarizes the effect of hydrostatic pressure on the stopping length of the streamer for various applied voltages in transformer oil.

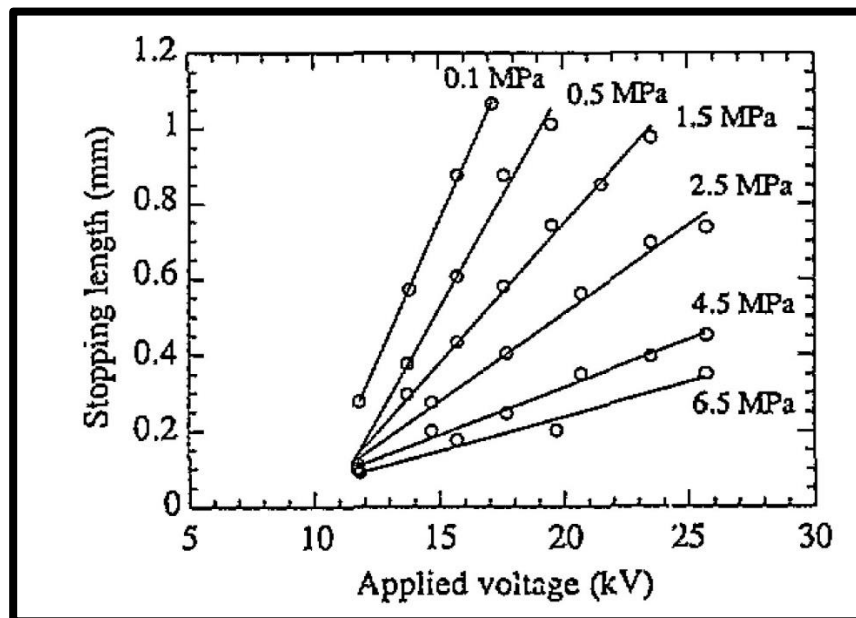


**Figure 7.** Results from Lesaint and Gournay showing the stopping length of arc streamers in transformer oil at various oil pressures with increasing applied voltage [8].

Lesaint and Gournay [8] suggests that a threshold exists where the method of streamer stopping shifts. At low pressures, the proposed method is that a voltage drop itself occurs inside the streamer. At high pressure, the higher pressure raises the boiling point of the dielectric, thus limiting bubble formation and enhancing bubble collapse, leaving no conductive material for the arc [8].

#### *Influence of Existing Lithotripsy Technology*

A lithotripter, a type of medical device, creates a high-pressure shockwave in the liquid water of the human body to break apart a kidney stone [9]. Utilizing technology similarly found

in lithotripters, the proposed breaker design uses a high-pressure shockwave to modulate the local density of the liquid dielectric between the electrodes of the spark gap in the arc chamber.

A shockwave is a sound wave. As a sound wave propagates, the medium's molecules experience compression and tension at various points in space. Equation 3 describes the total density of the medium in a sound wave, where  $\rho_{total}$  is the total density of the medium,  $\rho_{nom}$  is the density of the medium in the absence of the sound wave, and  $\rho_{var}$  is the change in density due to the sound wave [9]. Using the same subscripts, Equation 4 describes the pressure,  $P$ , of the sound wave [9]. Lastly, Equation 5 relates the change in density due to the sound wave to the change in pressure due to the sound wave, where  $c_0$  is the speed of sound in the liquid medium [9].

$$(3) \quad \rho_{total} = \rho_{nom} + \rho_{var}$$

$$(4) \quad P_{total} = P_{nom} + P_{var}$$

$$(5) \quad P_{var} = \rho_{var} c_0^2$$

The relative density perturbation is the ratio of the variable density to the nominal density of the liquid. For example, given water at 1000 kilograms per cubic meter with a sound speed of 1,500 meters per second, a relative density perturbation of five percent results in a sound pressure of approximately 112.5 MPa (16,317 psi) [9]. This means that a small compression of the liquid results in a sizable pressure wave.

#### *Methods of Pressure Wave Generation as Applied in Lithotripsy*

Three general lithotripter types generate high-pressure shockwaves in liquid. They are electrohydraulic, electromagnetic, and PZ. The technology behind these lithotripter devices is directly translatable to this breaker design. A summary of Cleveland and McAteer's comparison of the three generation types follows [9].

Electrohydraulic lithotripters create the high-pressure shockwave via a spark and focus the wave by an ellipsoidal reflector. Electrohydraulic lithotripters have a distinct disadvantage in that significant variability in the magnitude of the high-pressure wave from triggering event to triggering event may exist. As such, the electrohydraulic generation method is not ideal to the

proposed breaker design, because this shockwave generation method requires significant over-design to ensure that even in a worst-case scenario, the liquid pressure generated is high enough to satisfactorily raise the liquid's breakdown voltage and prevent or disrupt arc formation [9].

Electromagnetic shock generation uses an electric coil and a metal plate or membrane. A current pulse excites the coil, creating a magnetic force that vibrates the metal membrane and creates the high-pressure shockwave. This method produces consistent, reproducible pressure waves and does not require periodic electrode replacement [9]. Membrane wear over time could reduce the shockwave generator's effectiveness.

PZ shockwave generation requires application of a large differential voltage to a PZ transducer. Under the application of an opposing polarity voltage, the PZ transducer compresses. Following a rapidly applied matching-polarity voltage, the PZ transducer rapidly expands, creating a high-pressure shockwave [10]. Like electromagnetic shock generation, PZ shock generation produces consistent, reproducible pressure waves. Advantageously, it lacks a metal membrane that may wear out with time. Additionally, rapid switching of the applied voltage would allow for continuous, repetitive generation of high pressure. This ensures that a new wave maintains the high-pressure while the voltage transient during breaker operation settles [9]. All these factors considered; PZ transducers provide the most suitable means of high-pressure shockwave generation for this proposed breaker design.

Thomas, et al [11] conducted a lithotripsy experiment in which they tested various arrangements of PZ transducers to generate the high-pressure shockwave [11]. In an arrangement of three confocally-arranged PZ transducers and applying a charging voltage of 1.5 kV and discharge voltage of -16 kV, the degasified water under test experienced a maximum pressure of 40.9 MPa (5,932 psi) and minimum pressure of -16.9 MPa (-2,451 psi) over a period of approximately 2.5 microseconds as shown in Figure 8 [11].

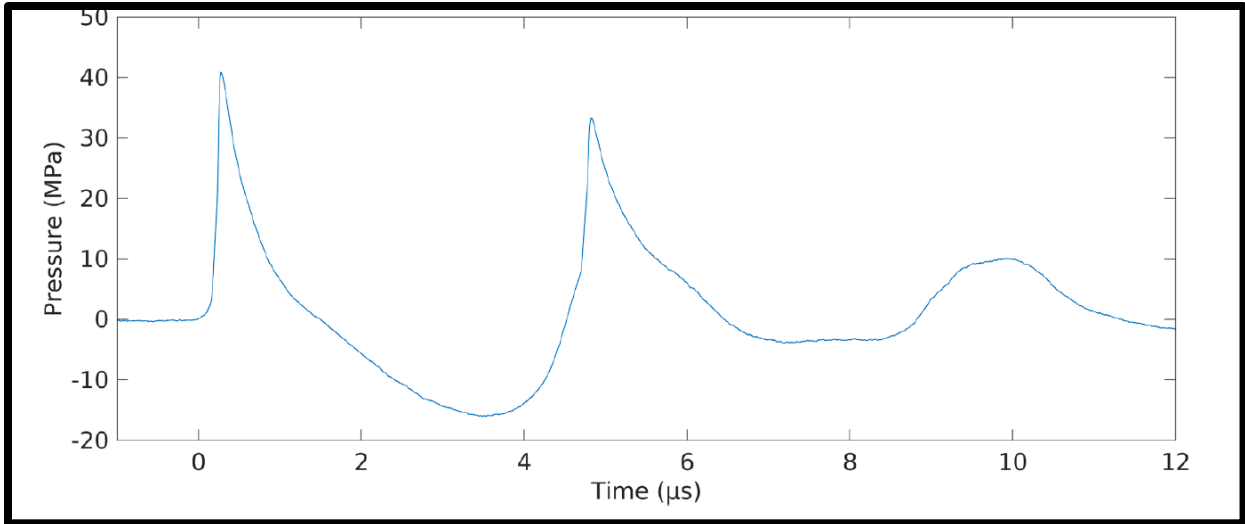


**Figure 8.** Resulting pressure shockwave from lithotripter testing by Thomas, et al [11]. Pressure oscillations occur as the pressure shockwave subsides. Positive pressures indicate compression of the liquid. Negative pressures indicate expansion of the liquid.

### Chapter 3: Development of Arc Transfer and Density Modulation Models

The following sections detail the development of the MATLAB/Simulink models used to assess the fundamental principles of the proposed breaker design.

#### *Arc Contact Transfer Model*

A MATLAB/Simulink model assesses the mechanism of arc transfer from the opening main breaker contacts to the arc chamber spark gap. Figure 9 shows the 60 Hz circuit in which a model simulates the Cassie arc model. Equation 6 describes the model circuit by Kirchoff's Voltage Law, where  $V_s$  is the source voltage, and the  $u$  term represents the arc voltage drop.

$$(6) \quad V_s = u - iR - L \frac{di}{dt}$$

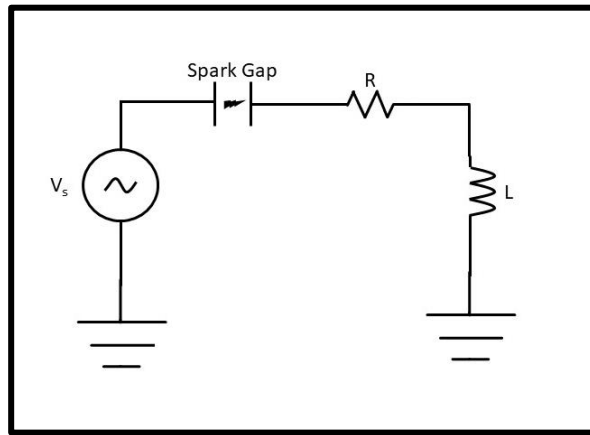


**Figure 9.** Generic circuit used to model a Cassie arc at 60 Hz.

Given that conductivity is the per-unit volume representation of conductance, the Cassie arc model may be re-written in terms of conductance ( $G_c$ ) as shown in Equation 7. Arc voltage may then be written in terms of arc current and conductance as shown in Equation 8. As such, the Cassie arc equation may be further re-written as shown in Equation 9.

$$(7) \quad \frac{1}{G_c} \frac{dG_c}{dt} = \frac{1}{\tau_c} \left( \frac{u^2}{U_c^2} - 1 \right)$$

$$(8) \quad u = \frac{i}{G_c}$$

(9) 
$$\frac{dG_c}{dt} = \frac{i^2}{U_c^2 \tau_c G_c} - \frac{G_c}{\tau_c}$$

The MATLAB/Simulink model shown in Figure 10 simultaneously solves Equations 6 and 9 to determine the arc current and the Cassie arc conductance. Figure 11 shows the specific Cassie arc conductance calculation.

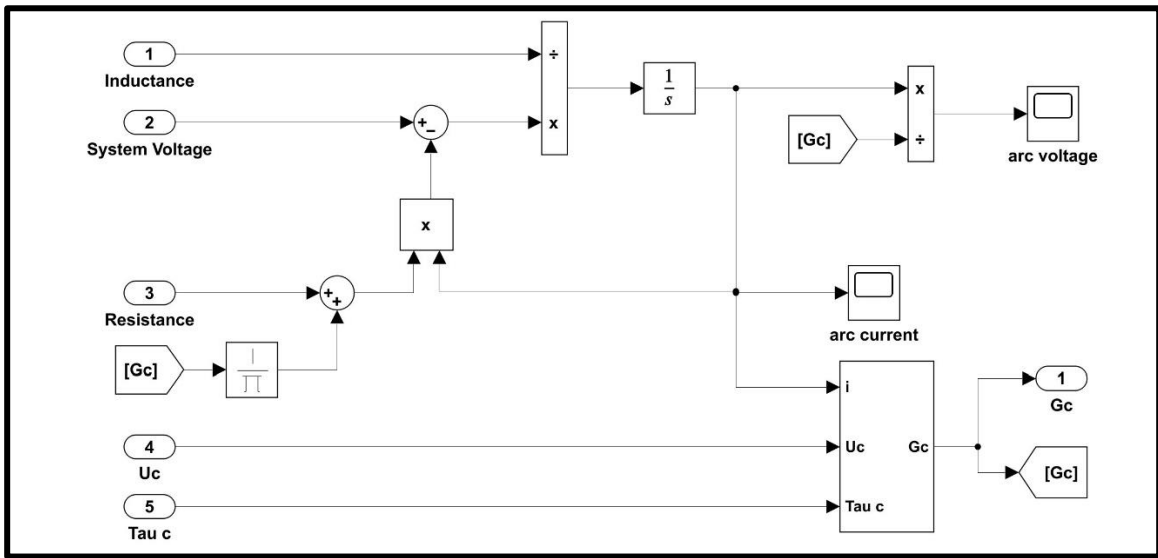


**Figure 10.** MATLAB/Simulink arc current, arc voltage, and Cassie conductance calculations.

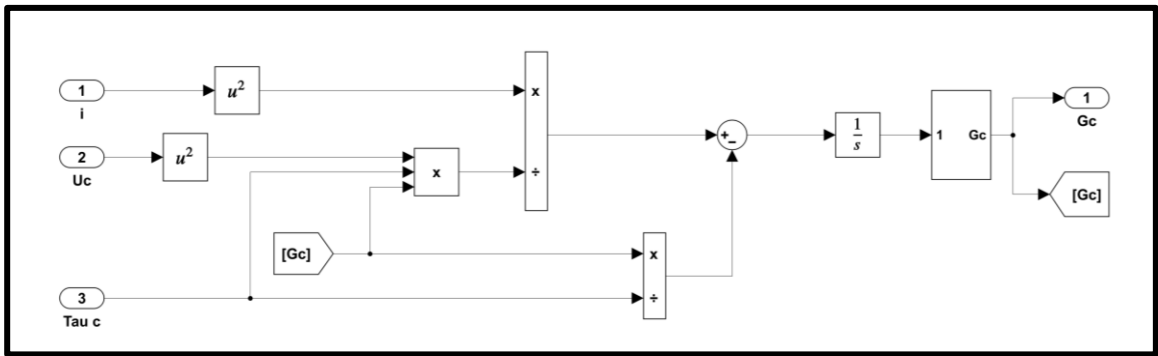


**Figure 11.** MATLAB/Simulink Cassie conductance calculation block.

As previously mentioned, a separating breaker contact can be modeled by increasing the arc voltage constant over time. After 0.05 seconds, the Simulink model increases the distance between the two contacts in the breaker at a rate of five millimeters (mm) per second starting from 0.1 mm. The starting distance was chosen to be greater than zero millimeters to operate under the assumption that the arc has already formed. The speed, intentionally slow compared to

a breaker which normally opens 10 or more millimeters in about 50 milliseconds, allows for better viewing of the results. The gap distance then enters a Lookup Table (LUT) to associate the gap distance with a voltage constant. The values in the LUT are estimations only and require laboratory experimentation, beyond the scope of this work, to verify.

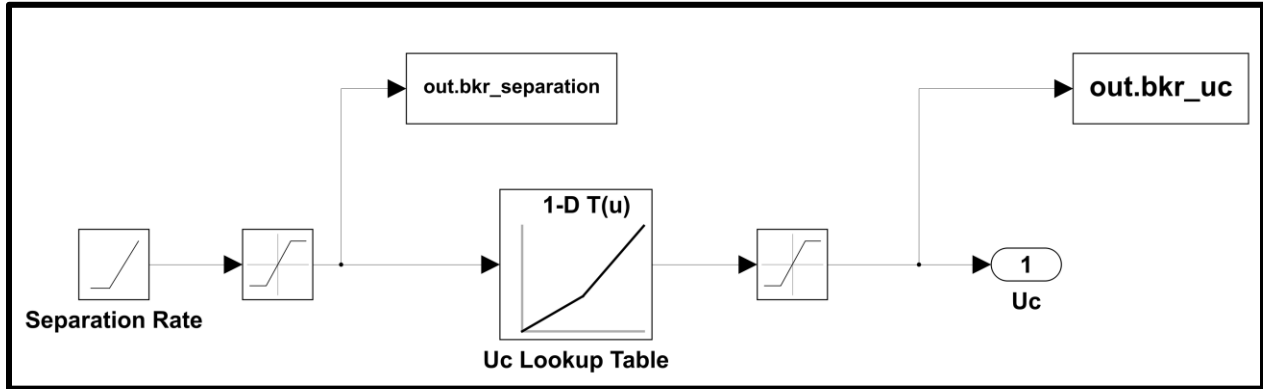


**Figure 12.** Cassie arc voltage constant determination.

*Density Modulation Simulation T&D Test System Parameters*

The model evaluated the feasibility of density modulation in a single-phase AC system with parameters as shown in Table 1. The appendix contains more information on single-phase fault and TRV analysis.

**Table 1.** T&D System Parameters for Breaker Response Simulation

Parameter	Value
Frequency	60 Hz
% Impedance (%Z)	8%
X/R Ratio	10
System Capacitance	1 $\mu$ F
Load Impedance	5 + j10 $\Omega$
Fault Impedance	0.001 $\Omega$

*Arc Chamber Model*

A separate MATLAB/Simulink model calculates the breakdown voltage in the arc chamber spark gap that results from a PZ transducer impulse. As outline in Figure 13, the model consists of three primary blocks: The Pressure Wave Generation Block, the Pressure-Density

Lookup Block, and the Density to Breakdown Voltage Block. The following sections detail the development and operation of the breakdown voltage calculation model.

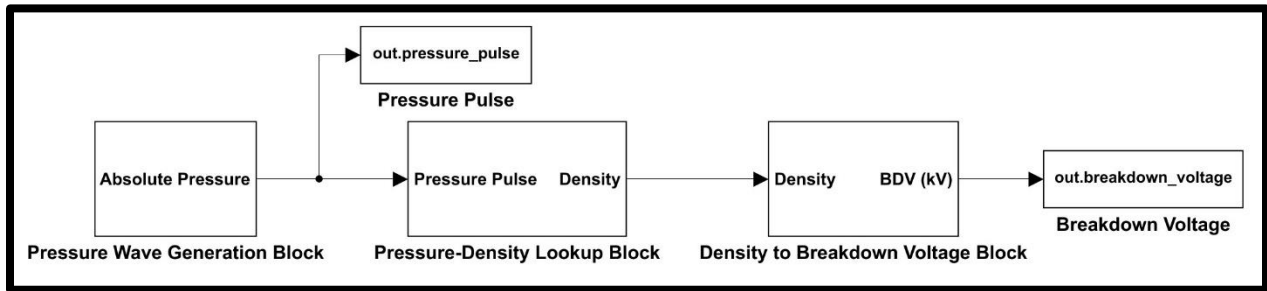


**Figure 13.** MATLAB/Simulink arc chamber spark gap breakdown voltage calculation model.

Before detailing the development of the density modulation model, the choice of liquid dielectric must first be addressed. The liquid dielectric chosen for the model is CO<sub>2</sub>. However, liquid CO<sub>2</sub> is non-ideal for the proposed breaker application. CO<sub>2</sub> only exists in liquid form over a limited temperature range, approximately -56°C to 31°C [12]. This means that the arc chamber must be maintained very cold or highly pressurized to keep the CO<sub>2</sub> in liquid form. This model places the CO<sub>2</sub> to be under high pressure. Despite these non-idealities, this simulation uses liquid CO<sub>2</sub> because previous research by Young provides usable data relating density, a function of fluid temperature and pressure, to breakdown voltage [6]. The results of Lesaint and Gournay previously discussed detailing the relationship between stopping length and applied voltage at various pressures demonstrate that a liquid like transformer oil may possess the needed dielectric qualities for this breaker application with phase stability at standard temperature and pressure [8]. As so, the qualities of an ideal liquid dielectric for this breaker application are detailed later in this paper.

In the subcooled state, there are two primary means of affecting density of a liquid. One is to increase the pressure. The other is to decrease the temperature. Because of the rapidity at which this change in density change must occur in the arc chamber to provide a timely protective action response, this model uses pressure the means to manipulate density. Pressure sources such as air tanks, or in this case PZ transducers, chosen for their pressure pulse consistency and repeatability, can instantly apply high compressive pressures. To use temperature would require a significant amount of instantaneous heat transfer that is not practical.

## Pressure Wave Generation Block

The Pressure Wave Generation Block (PWGB), shown in Figure 14 computes the local pressure in the arc chamber spark gap. The model assumes a similar three PZ transducer confocal setup as used by Thomas, et al [11]. Positive charging and negative discharging PZ transducer voltages, liquid CO<sub>2</sub> holding pressure, and the pressure decay slope are the primary inputs to the PWGB. Step insertions sequence the primary pressure pulse and its subsequent oscillations. The following sections detail each input, assumption and calculation.

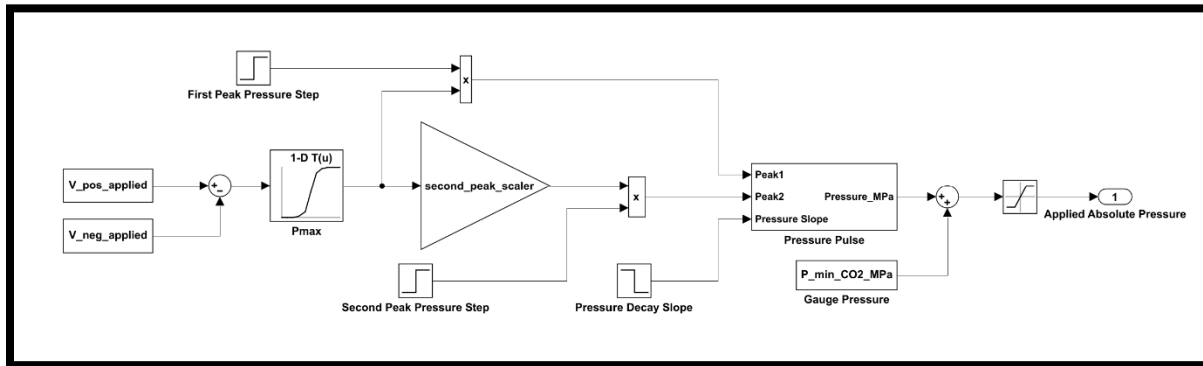


**Figure 14.** Simulink model of the Pressure Wave Generation Block.

The difference between positive charging and negative discharging voltages of the PZ transducers determines the magnitude of the maximum gauge pressure, or pressure above the holding pressure of the liquid CO<sub>2</sub>, from the transducer array. This differential voltage then enters a LUT that outputs the maximum positive pressure generated by the array based on the applied differential voltage. Citing Thomas, et al and the limitations of the equipment associated with their testing, the maximum applied differential voltage is 17.5 kV because physical damage may occur to the transducers above that voltage [11].

Data from Thomas's previous work, as shown in Figure 15, provides a basis for modeling the pressure pulse at differential voltages less than 17.5 kV [11]. Using a four-transducer confocal setup, Thomas, et al showed that when applying 80% of maximum differential voltage, the peak pressure achieved is only 55% of the peak pressure that occurs at full voltage [11]. Also noteworthy, the general shape and slope of the pressure decay is similar between the two different voltages. As such, the model assumes a pressure decay slope independent of the applied differential voltage.

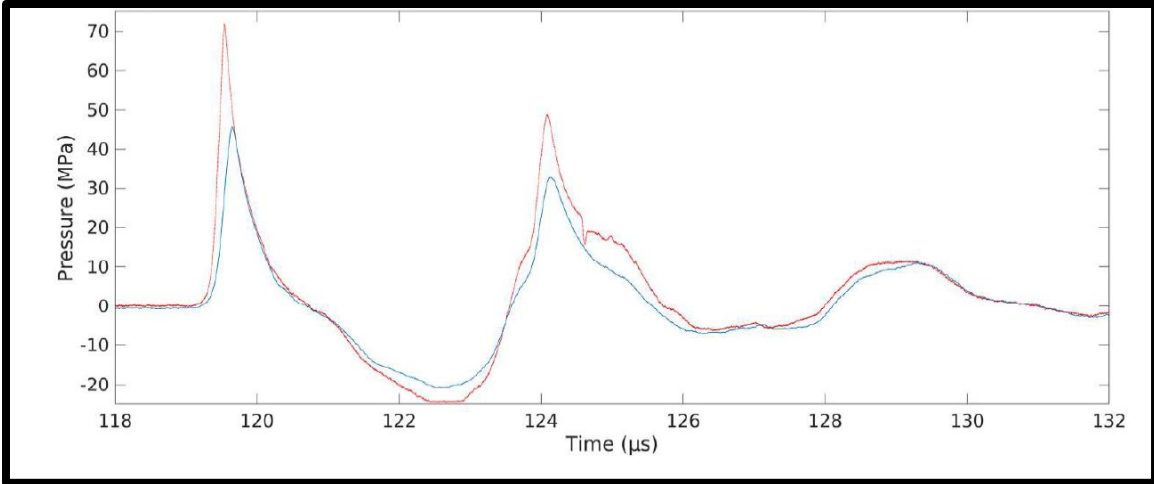


**Figure 15.** Thomas, et al experimental results comparing pressure response when applying maximum differential voltage (red) versus 80% differential voltage (blue) [11].

Extrapolating the four-transducer results to the three-transducer setup in this model creates the maximum pressure LUT, as shown in Figure 16. The general shape of the curve in the LUT suggests a squared relationship. Because transducers are capacitive in nature, the energy stored in the charging and discharging capacitors of the PZ transducer circuit is proportional to the square of voltage. Smaller incremental changes in voltage result in larger energy storage. More energy results in a larger force and therefore a larger pressure.

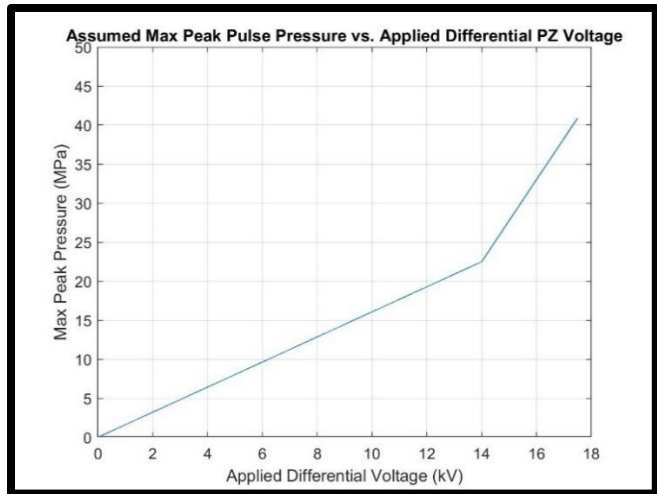


**Figure 16.** Maximum peak pressure versus applied differential voltage.

Additionally, the model assumes that liquid CO<sub>2</sub> and the previous experimenters' medium have similar speeds of sound, resulting in similarly shaped shockwaves [11]. For

simplicity, the model assumes vertical pressure rises to peak pressure and linear pressure decay. The model also neglects tertiary and greater oscillations as demonstrated in Thomas's research [11]. The overall result from the model is an asymmetrical sawtooth-like pulse created by the first pressure peak, second pressure peak, and pressure decay slope step inputs. The minimum pressure is limited to 0.01 MPa, because National Institute of Standards and Technology (NIST) reports the density of CO<sub>2</sub> as zero grams per milliliter (g/ml) at zero MPa [12]. Limiting the minimum pressure to slightly above zero MPa ensures a measurable density.

The last input is the steady state holding pressure of the liquid CO<sub>2</sub>, also referred to as  $P_{nom}$  previously in Equation 2. In this model, the steady state pressure is the minimum pressure at which CO<sub>2</sub> exists in liquid form at a given temperature. This pressure must be applied by an external source such as an air flask or piston. This study does not model such an external force. The PWGB sums the variable pressure applied by the PZ transducer and steady state holding pressure to generate the applied absolute local pressure in the arc chamber spark gap. Laboratory verification would validate the summation of the steady state holding pressure and the variable pressure applied by the PZ transducer. Figure 17 shows an example of a pressure pulse that results from the PWGB. This pressure output passes into the Pressure-Density Lookup Block.

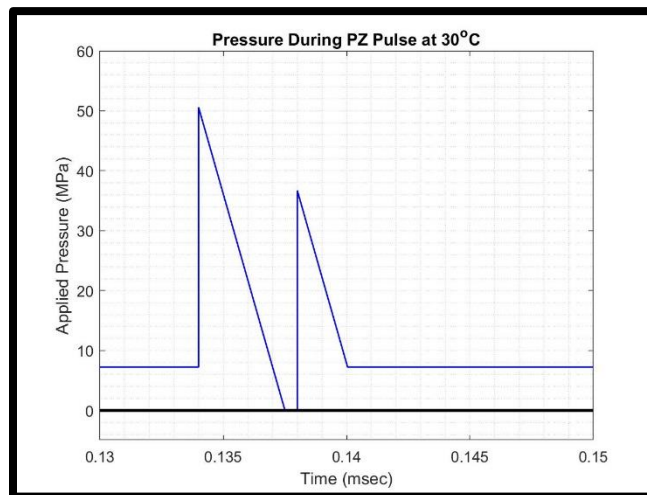


**Figure 17.** Example of an asymmetrical pressure pulse generated by the PWGB peak pressure calculations.

### Pressure-Density Lookup Block

The output of the Pressure Wave Generation Block passes into the Pressure-Density Lookup Block (PDLB). The PDLB makes several assumptions to account for the non-idealities

of liquid CO<sub>2</sub> and the shape of the pressure waveform. First, the block neglects the temperature effects from liquid compression and arc heating. This means that the liquid CO<sub>2</sub> does not flash into vapor from temperature variation. Second, as the pressure wave generates negative pressures from the expansion of the liquid after the shock, the model limits the minimum density to that associated with 0.01 MPa. This implies that a low enough pressure may occur during the liquid's expansion that the liquid CO<sub>2</sub> flashes to gas, resulting in very low-density CO<sub>2</sub> in the arc chamber spark gap. This transition occurs near-instantaneously at the saturation pressure, resulting in a sharp downturn in CO<sub>2</sub> density at low pressure, as shown in Figure 18.

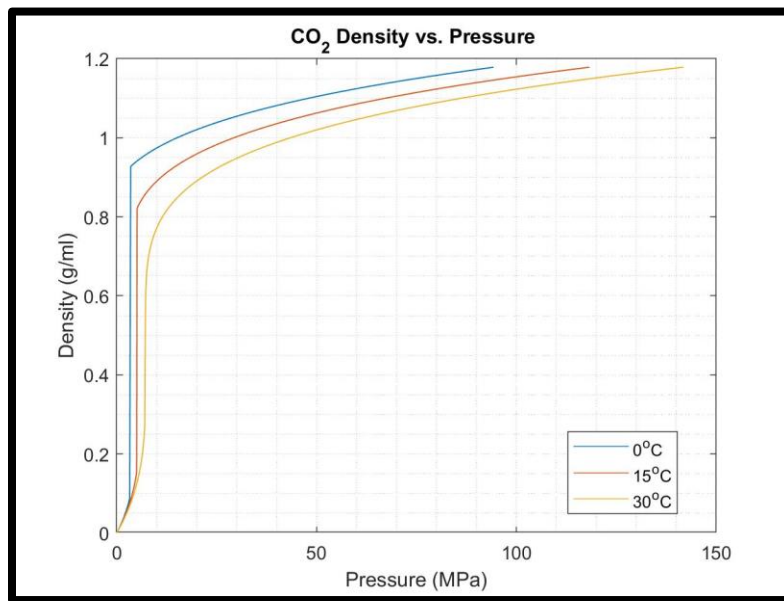


**Figure 18.** Density of CO<sub>2</sub> versus pressure at 0°C, 15°C, and 30°C. The knee in each curve indicates the transition from gaseous to liquid form with increasing pressure [12].

At higher temperatures, the density of liquid CO<sub>2</sub> occupies a wider range. Consequently, at higher temperature the holding pressure of the CO<sub>2</sub> must be higher. Achieving a lower liquid density may prove important to the arc transfer mechanics from the main breaker contacts to the arc chamber.

This block contains a LUT that references the pressure of CO<sub>2</sub> at a given temperature to the density as provided by NIST which reports the maximum achievable density of liquid CO<sub>2</sub> as 1.1785 g/ml [12]. This maximum provides the upper limit to a saturation block as shown in Figure 19. The PDLB outputs a density to the Density to Breakdown Voltage Block.

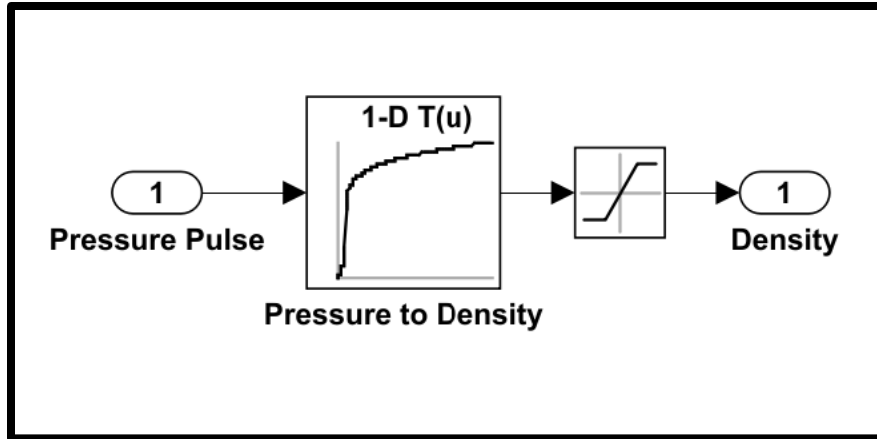


**Figure 19.** Pressure-Density Lookup Block.

Density to Breakdown Voltage Block

The Density to Breakdown Voltage Block (DBDVB), shown in Figure 20, receives a density input from the Pressure-Density Lookup Block and outputs the breakdown voltage of the liquid CO<sub>2</sub> resultant of the shockwave induced density modulation. The LUT in the DBDVB references density to experimental data obtained by Young [6].

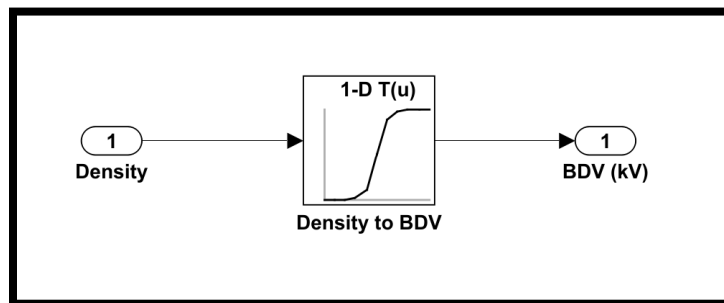


**Figure 20.** Density to Breakdown Voltage Block

Young’s data, extracted using a MATLAB script by Cheung, only provides data to about 0.7 g/ml [6], [13]. As previously mentioned, liquid CO<sub>2</sub> exists at a density of up to 1.1785 g/ml. As such, the LUT assumes a linear relationship between density and breakdown voltage above 0.7 g/ml, as shown in Figure 21. This is purely an assumption and requires validation through laboratory experimentation, beyond the scope of this work. This block assumes a 0.0075-inch spark gap distance, maintaining consistency with Young’s setup [6].

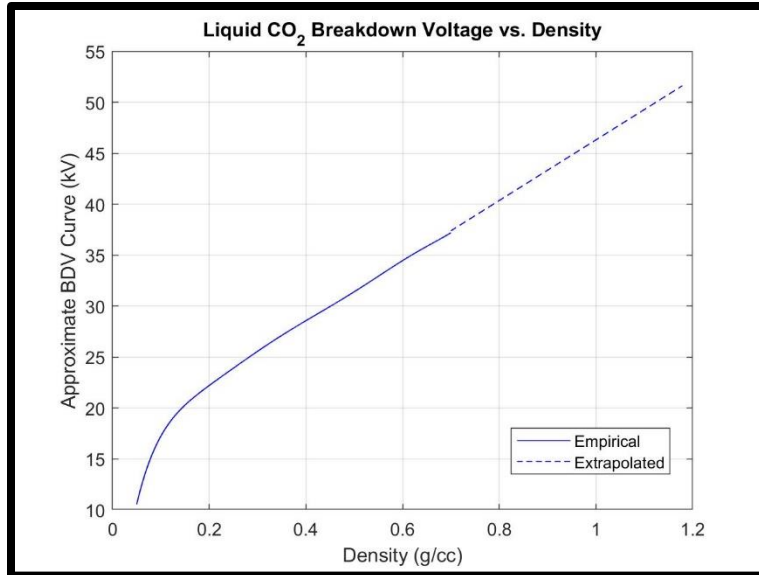


**Figure 21.** LUT contains a synthesis of Young's experimental results with a linearly extrapolated results above 0.7 g/ml [6].

## Chapter 4: Results and Discussion

The following section details the results of the arc transfer and PZ pulse simulations and provides commentary on the significance and implications of these findings.

### *Arc Transfer Simulation Results and Discussion*

This section compares the results of two simulations of the Cassie arc model in the circuit previously described. The first simulation analyzed an arc gap with a fixed electrode separation of 0.2 mm. The second simulation analyzed a moving arc gap that started at 0.1 mm and expanded at a rate of five millimeters per second. Figure 22 shows compares the stationary arc gap distance to the expanding arc gap distance. Figure 23 shows the changing arc voltage constant over time that results from the expanding distance between breaker contacts. Finally, Figure 24 shows the arc conductance versus time comparing the fixed spark gap to the expanding gap between the breaker contacts.

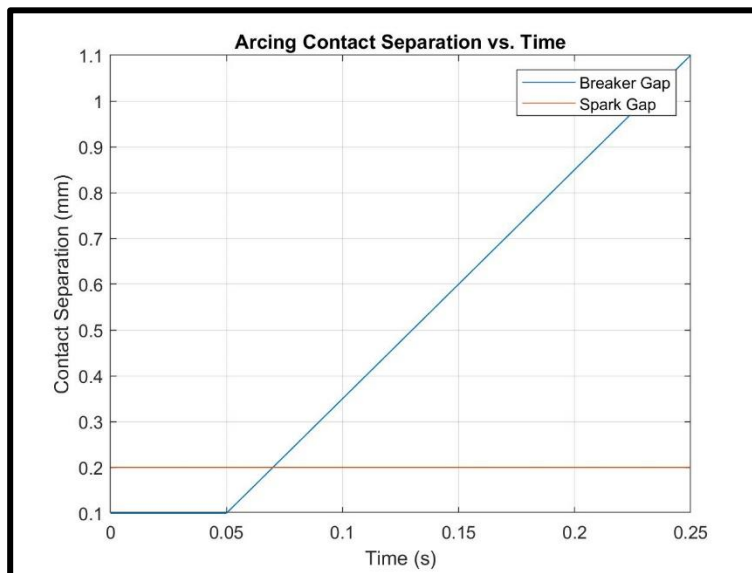


**Figure 22.** Arc contact separation versus time.

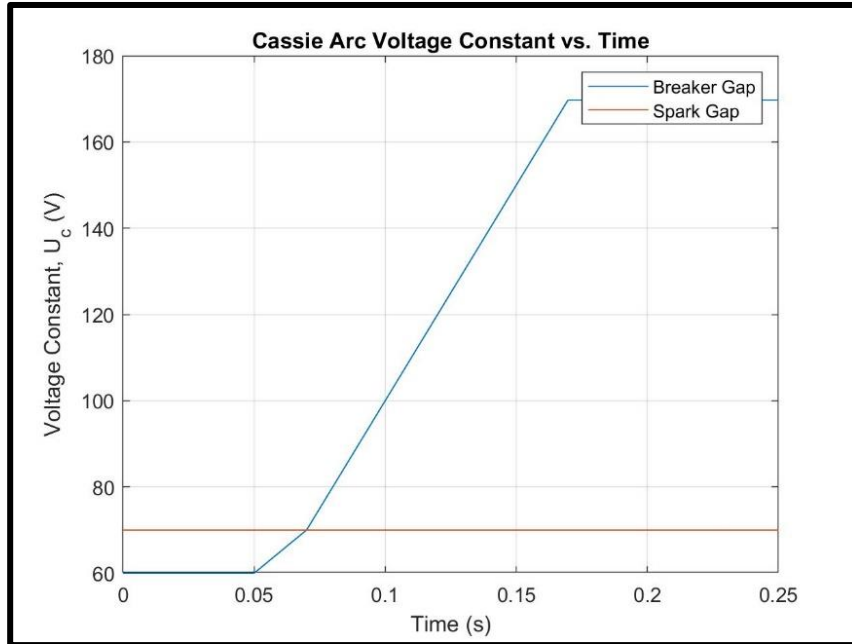


**Figure 23.** Arc voltage constant versus time.

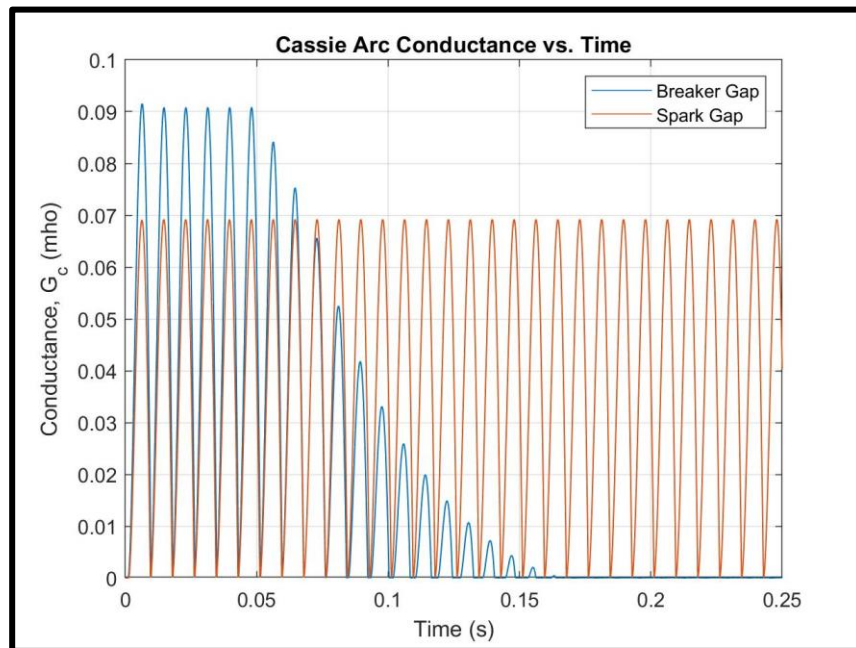


**Figure 24.** Cassie arc conductance versus time.

The breaker contacts begin to separate beyond 0.1 mm after 0.05 seconds into the simulation. As shown in Figure 24, the conductance between the breaker contacts equals the conductance of the fixed spark gap at 0.07 seconds. At this point, the spark gap is more conductive, meaning that more arc current will flow to the spark gap. Around 0.15 seconds, the

breaker contacts open far enough that the conductance between the breaker contacts is zero, meaning that all current is flowing through the spark gap. This would be when the PZ pulse mechanism actuates to extinguish the arc.

The results of this simulation suggest that the arc would transfer from the breaker contacts to the arc chamber with time. However, the results of this simulation require verification through laboratory experimentation.

### *Density Modulation Simulation Results and Discussion*

In the simulation, the breaker opened in response to a bolted line-to-ground fault at the worst point-on-wave. The maximum TRV achieved was approximately twice the source voltage. On the rising TRV, the breaker applies a single pressure pulse to the arc chamber.

This study evaluated density modulation with respect to three different sensitivities: CO<sub>2</sub> liquid temperature, applied PZ transducer voltage, and system level voltage and apparent power. In these three cases, all other parameters remained unchanged. Of note, in all simulations, breakdown voltage oscillates because of pressure oscillations from the PZ pulse. These oscillations are explained by the liquid rapidly expanding after the pulse. Pressure may drop low enough during expansion to cause the liquid CO<sub>2</sub> to flash to vapor momentarily before the fluid begins to go through another positive pressure oscillation, causing rapid condensation.

### Sensitivity to Different Liquid CO<sub>2</sub> Temperature

Simulation of various temperatures of the liquid CO<sub>2</sub> provides insight into desirable fluid properties for use in real-world development of this breaker. Simulation results show that maintaining the CO<sub>2</sub> at higher temperatures allows larger density modulation, which results in a difference between steady state breakdown voltage and peak breakdown voltage during breaker operation. Table 2 briefly summarizes the significant fluid properties assessed during simulation at 0°C, 15°C, and 30°C with system voltage, apparent power, and peak pulse voltage at 13.1 kV, 20 MVA, and 17.5 kV differential, respectively.

**Table 2.** Summary of Temperature Sensitivity Results

	0°C	15°C	30°C
<b>Resting Pressure (MPa)</b>	3.4851	5.0871	7.2317
<b>Resting Density (g/cc)</b>	0.9274	0.8212	0.5933
<b>Resting BDV (kV)</b>	44.1558	40.9976	34.2696
<b>Peak Pressure (MPa)</b>	44.3851	45.9871	48.1137
<b>Peak Density (g/cc)</b>	1.0919	1.0523	1.0145
<b>Peak BDV (kV)</b>	49.0467	47.8675	46.7436
<b>Density Modulation (<math>\rho_{\text{peak}}/\rho_{\text{resting}}</math>)</b>	1.1744	1.2814	1.7098

Because the resting BDV is always above the TRV in the 0°C case as shown in Figure 25, an arc will likely not form in the spark gap. This means that the main breaker contacts must endure the arc, rather than allowing the arc to transfer to the spark gap in the arc chamber. Therefore, the breaker requires a lower steady state BDV, (i.e., a lower steady state liquid density). Maintaining the liquid CO<sub>2</sub> at a higher temperature achieves this end.

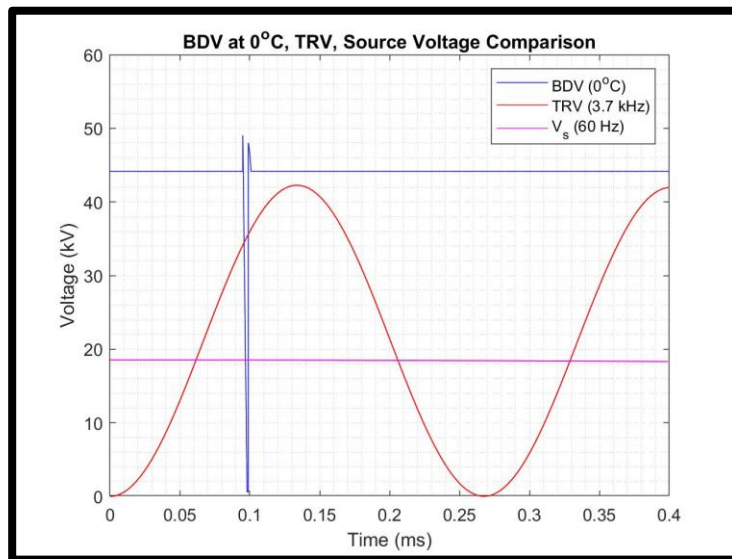


**Figure 25.** BDV in the arc chamber spark gap, TRV, and source voltage as a function of time with 0°C liquid CO<sub>2</sub>.

Figure 26 shows the results of the arc chamber simulation with the liquid CO<sub>2</sub> at 15°C. In this case, the TRV does not exceed the steady state BDV until nearly the peak of the TRV occurs. This would delay arc transfer from the breaker contacts to the arc chamber.

Consequently, this potentially subjects the main breaker contacts to an arc for an extended duration.

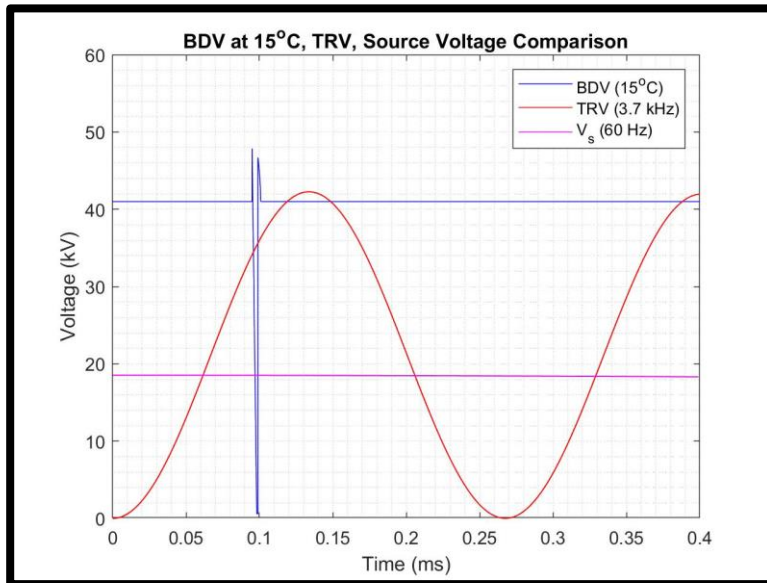


**Figure 26.** BDV in the arc chamber spark gap, TRV, and source voltage as a function of time with 15°C liquid CO<sub>2</sub>.

Figure 27 shows the results of the final temperature sensitivity simulation case with the liquid CO<sub>2</sub> temperature at 30°C. Compared to the 15°C case, the TRV exceeds the BDV in the arc chamber sooner. This enables the arc to transfer sooner, subjecting the main breaker contacts to less wear. Once again, it must be reiterated that 30°C is the practical limit for the existence of CO<sub>2</sub>. Temperature variations that may occur from arc heating could cause the liquid CO<sub>2</sub> to flash, severely dropping the breakdown voltage and likely resulting in a significant arc that may continue when open circuit voltage is achieved.

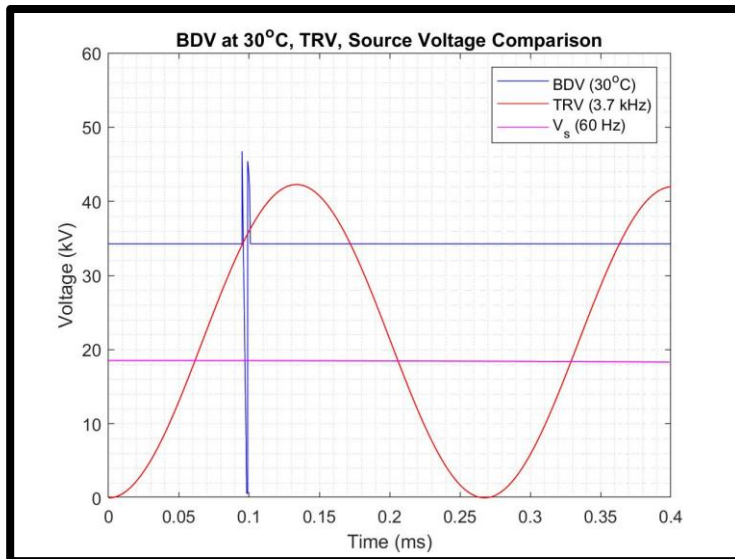


**Figure 27.** BDV in the arc chamber spark gap, TRV, and source voltage as a function of time with 30°C liquid CO<sub>2</sub>.

It is important that the resting BDV always remains higher than the nominal source voltage in all cases. This ensures that when the breaker is in an open state, such as for maintenance or other switching operations, an arc will not form in the arc chamber spark gap, conducting current down the line to loads. Additionally, a system commissioned in real-world application would likely desire a larger margin between peak TRV and maximum achieved breakdown voltage. Follow on pulses would be also likely be required to ensure that the pressure pulse achieves a standing waveform that remains above the TRV as the transient subsides, preventing re-ignition of the arc.

### Sensitivity to PZ Voltage

Sensitivity to PZ voltage provides insight into the energy storage and sizing requirements of charging capacitors in the PZ transducer circuit. As expected, simulation results show that higher applied differential voltages across the PZ transducer produce higher peak pressures. Higher differential voltages therefore result in greater density modulation, and subsequently, higher breakdown voltages. Table 3 briefly summarizes the significant fluid properties assessed during simulation at applied differential voltages of 13.5 kV, 15.5 kV, and 17.5 kV with CO<sub>2</sub> temperature, system voltage, and apparent power at 30°C, 13.1 kV, and 20 MVA, respectively. The largest differential voltage applied corresponds to the maximum differential voltage that can be applied to the transducers used by Thomas, et al.

**Table 3.** Summary of Applied PZ Voltage Sensitivity Results

	13.5 kV	15.5 kV	17.5 kV
<b>Resting Pressure (MPa)</b>	7.2317	7.2317	7.2317
<b>Resting Density (g/cc)</b>	0.5933	0.5933	0.5933
<b>Resting BDV (kV)</b>	34.2696	34.2696	34.2696
<b>Peak Pressure (MPa)</b>	28.9053	37.5966	48.1137
<b>Peak Density (g/cc)</b>	0.9428	0.9796	1.0145
<b>Peak BDV (kV)</b>	44.6122	45.7069	46.7436
<b>Density Modulation (<math>\rho_{\text{peak}}/\rho_{\text{resting}}</math>)</b>	1.5890	1.6511	1.7098

The following three figures graphically represent the results of the arc chamber simulations at various applied differential voltages across the PZ transducer array. Figure 28 displays the 13.5 kV case, Figure 29 shows the 15.5 kV case, and Figure 30 shows the 17.5 kV case. The peak BDV achieved across each simulation is very similar.

The difference between the 13.5 kV and 17.5 kV test cases is only about 2.1 kV. With such a small difference, it may prove advantageous to operate at lower applied differential voltages. This means that the energy capacitively stored in the PZ transducer would be less, reducing the charging time required and making repeat pulse operation more feasible. Additionally, the lower voltage would reduce wear on the PZ transducers.

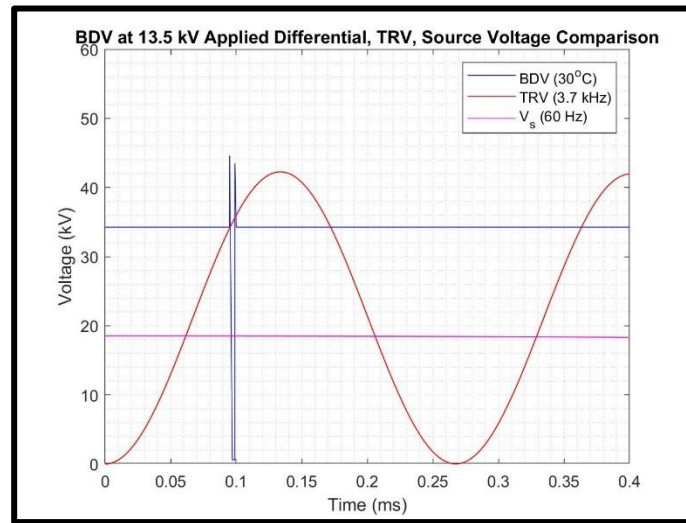


**Figure 28.** BDV in the arc chamber spark gap, TRV, and source voltage as a function of time when 13.5 kV is applied across the PZ transducer array.

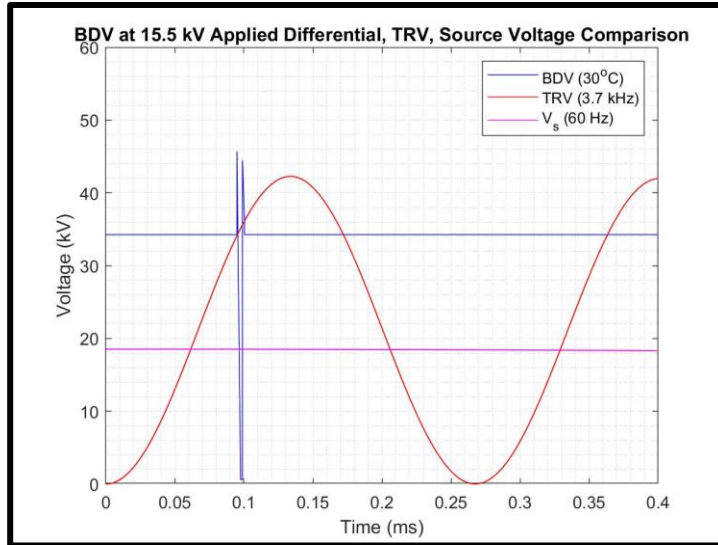


**Figure 29.** BDV in the arc chamber spark gap, TRV, and source voltage as a function of time when 15.5 kV is applied across the PZ transducer array.

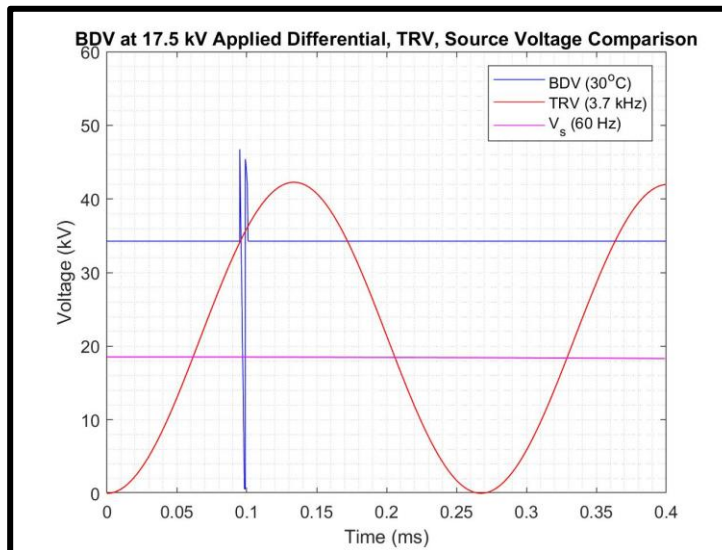


**Figure 30.** BDV in the arc chamber spark gap, TRV, and source voltage as a function of time when 17.5 kV is applied across the PZ transducer array.

### Sensitivity to System Voltage

Simulation results varying the system voltage and apparent power provide insight into establishing ratings for this breaker design. Simulations analyzed in this case are at 7.2 kV and 10 MVA, 13.1 kV and 20 MVA, and 33 kV at 40 MVA. The following figures show the results of this simulation. These results are largely dependent on the electrode spark gap. This study

assumed a 0.0075-inch spark gap. As seen in the 7.2 kV and 10 MVA case, the BDV in the gap is too large. Higher voltage systems would require a large arc chamber spark gap to maintain a sufficiently high breakdown voltage.

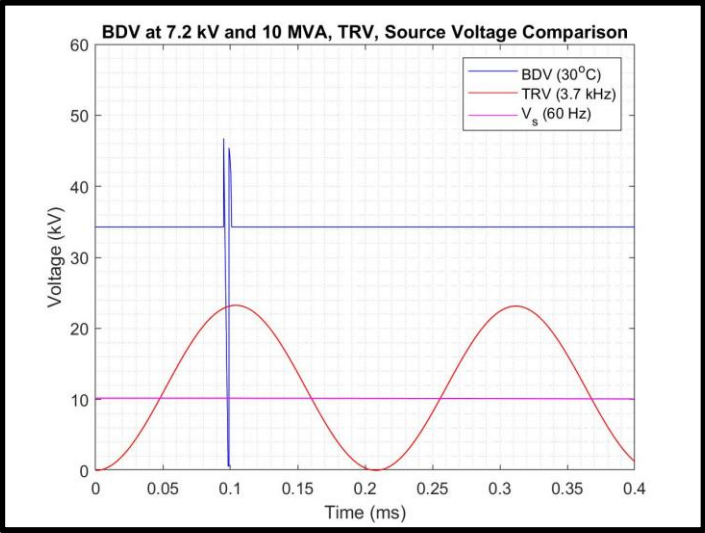


**Figure 31.** BDV in the arc chamber spark gap, TRV, and source voltage as a function of time when system voltage and apparent power are 7.2 kV and 10 MVA, respectively.

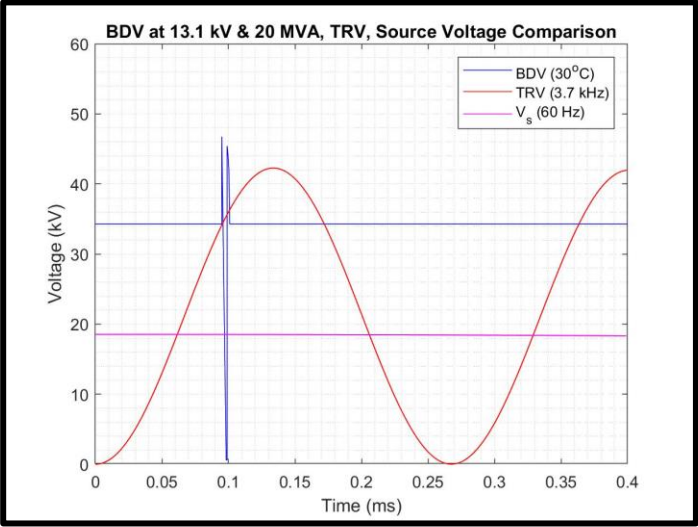


**Figure 32.** BDV in the arc chamber spark gap, TRV, and source voltage as a function of time when system voltage and apparent power are 13.1 kV and 20 MVA, respectively.

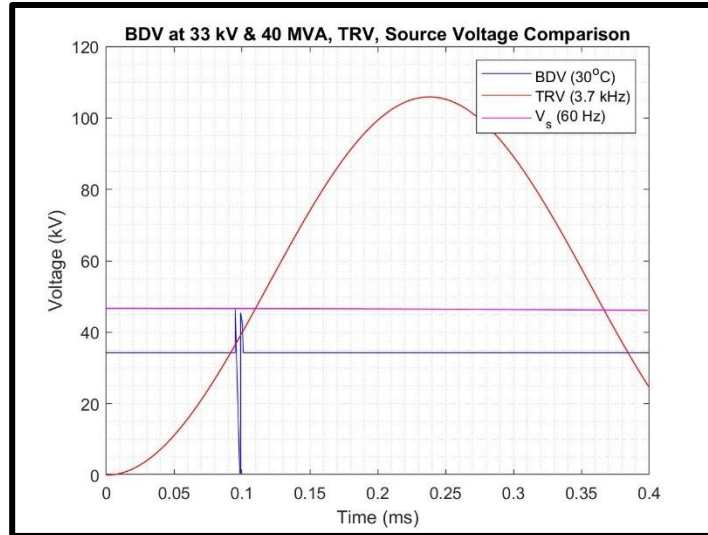


**Figure 33.** BDV in the arc chamber spark gap, TRV, and source voltage as a function of time when system voltage and apparent power are 33 kV and 40 MVA, respectively.

#### *Comparison to SF<sub>6</sub> and Other Gaseous Insulators*

Though SF<sub>6</sub> demonstrates deficiencies related to greenhouse gas emissions, gas insulating breaker technology still serves as the standard of comparison for new breaker designs. One distinct advantage of SF<sub>6</sub>, and all gaseous insulators for that matter, is the more uniform pressure distribution in the arcing chamber. When the gas enters the arcing chamber, it spreads more uniformly than a liquid. This means that the entire chamber is subjected to the arc-quenching characteristics of the gas, as compared to the small area of high pressure generated by the PZ transducers in liquid.

Other investigations also allow for comparison to SF<sub>6</sub> and other gaseous insulators. With increasing pressure and spark gap distance, the breakdown voltage of SF<sub>6</sub> increases. From Figure 34, a similarly sized SF<sub>6</sub>-filled spark gap of 0.0075 inches pressurized to 0.6 MPa (87 psi) results in a breakdown voltage of approximately 10 kV [14]. This breakdown voltage is substantially lower than the breakdown voltages calculated in the liquid CO<sub>2</sub> breaker model. By increasing the spark gap distance, the breakdown voltage of SF<sub>6</sub> rises linearly, allowing SF<sub>6</sub> to achieve comparable breakdown voltages calculated by the liquid CO<sub>2</sub> breaker. These comparable breakdown voltages occur at gap distances of approximately one millimeter, approximately five times the gap length in this paper's simulation. These larger gap distances allow easier construction and experimentation.

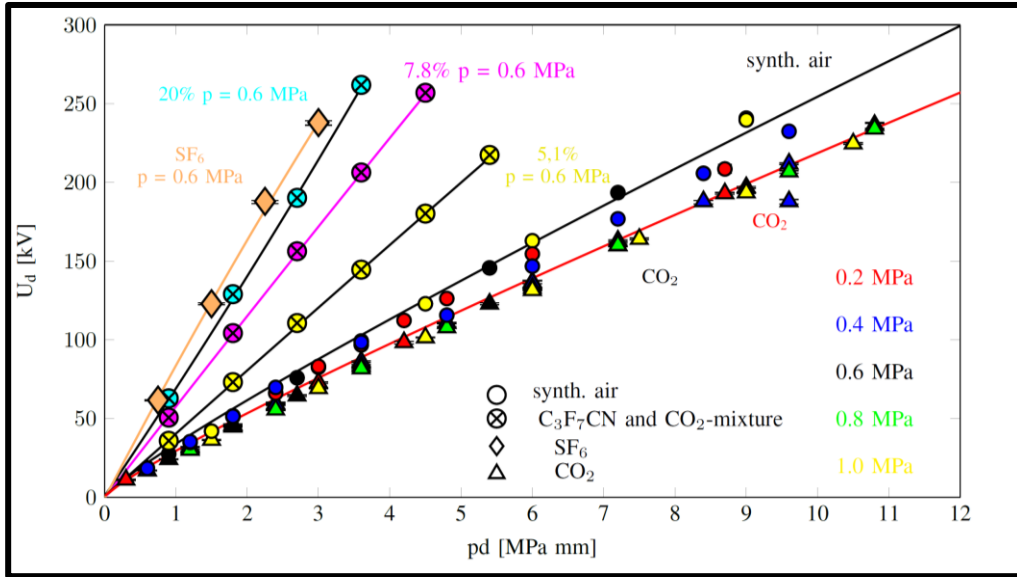


**Figure 34.** BDV's for various gases with respect to pressure and gap distance [14].

Shown in Figure 35, SF<sub>6</sub> dielectric strength increases with gas pressure. Similarly, gaseous CO<sub>2</sub> is shown to have increased dielectric strength with increasing gas pressure. Albeit the dielectric strength of SF<sub>6</sub> is significantly higher than that of gaseous CO<sub>2</sub>. The positively increasing dielectric strength of SF<sub>6</sub> and other gaseous insulators with gas pressure continues to suggest that higher pressure induces greater breakdown voltages, supporting the hypothesis that the hypothesis that the same effect occurs in liquid insulators such as CO<sub>2</sub>.

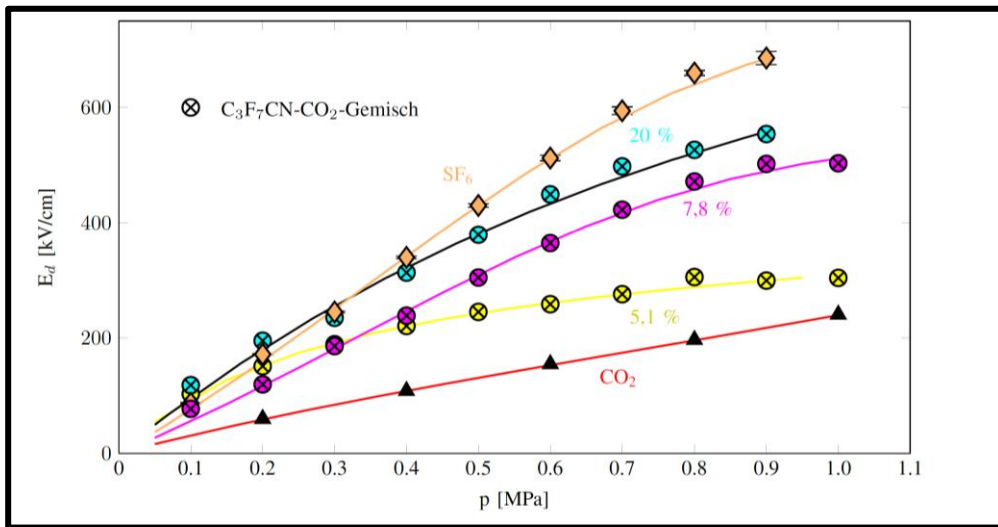


**Figure 35.** Relationship between dielectric strength and gas insulator pressure [14].

Overall, the combination of previous investigations by researchers such as Young and the current work show that liquid insulators, such as CO<sub>2</sub>, demonstrate increased dielectric strength and breakdown voltage with increased pressure. This relationship neatly parallels pressure, dielectric strength, and breakdown voltage relationships in gaseous insulators. The most significant challenge to comparable performance of the liquid insulator breaker to the gas insulator breaker is achieving uniform dielectric properties over the entire area the arc occupies.

## Chapter 5: Additional Considerations

This work noted that several assumptions of the liquid CO<sub>2</sub> breaker model require laboratory experimentation for verification. A few of these required validations include the Cassie arc voltage constant relationship with arc gap distance, pressure/density response of the dielectric liquid to the PZ pulse, and breakdown voltage response to CO<sub>2</sub> density greater than 0.7 grams per centimeter (<sup>g</sup>/<sub>cc</sub>).

While these experiments would validate and/or reject the models or their parts, several design challenges, investigations, and considerations remain before even prototype development of the liquid breaker. Specifically, these include challenges such as dielectric medium selection, fault response, and PZ transducer actuation timing. Beyond prototype development, failure modes for this breaker must be considered. This section briefly considers these future considerations and investigations.

### *Dielectric Medium Selection*

Investigation into a suitable liquid dielectric for this breaker remains an open avenue of research. As mentioned previously, liquid CO<sub>2</sub> is non-ideal for this breaker application. A suitable dielectric for this breaker design would be a liquid which exists over a wide temperature and pressure range and demonstrates slight compressibility. The liquid dielectric should ideally exist in liquid form at atmospheric pressure and environmental temperatures exceeding 200°C to withstand both environmental and arc heat. Slight compressibility allows for slight modulation of the breakdown voltage. For example, at 30°C and between 7.25 MPa (1,052 psi) and 141.53 MPa (20,525 psi), the density of liquid CO<sub>2</sub> varies from 0.61258 to 1.1783 <sup>g</sup>/<sub>ml</sub>. By comparison, water at the same temperature and over the same pressure range varies from 0.9988 to 1.048 <sup>g</sup>/<sub>ml</sub> [12]. Liquids such as transformer oil or mineral oil provide suitable starting points for this investigation. Further research may prove that a novel liquid dielectric is necessary and must be developed.

### *Fault Response and PZ Transducer Timing Considerations*

Timing systems for the liquid insulating breaker encompass several categories of challenges. These include challenges include fault detection and breaker actuation, PZ transducer pulse, and PZ transducer recharge.

Fault detection and breaker actuation relies on traditional fault sensing techniques such as undervoltage relays, ground relays, and current transformers. A system must be designed to quickly determine a fault and begin the breaker actuation process.

The timing of the PZ transducers provides a more detailed design challenge. First, the arc must sufficiently transfer from the main breaker contacts to the arc chamber before pulsing the PZ transducer. This may be accomplished by using a photosensor to detect the arc in the chamber. If the PZ pulse occurs before the arc transfers, the breakdown voltage in the spark gap may rise to a value high enough preventing arc transfer entirely, meaning that the main breaker contacts must endure the full wear of the arc. The breaker contacts must also open sufficiently that at the time of the PZ pulse, the arc does not restrike across the main breaker contacts.

Practical application of this breaker design would require repeated pulses of the PZ array to maintain the breakdown voltage in the spark gap high enough during the TRV to prevent restrike, effectively creating a standing pressure wave in the arc chamber spark gap. This could be accomplished by using an array of PZ transducers that pulse in sequence, repeatedly charging and pulsing PZ transducers, or a combination of both. Figure 36 provides a conceptual drawing of PZ arrangements to achieve this goal. Arrangement A repeatedly charges and discharges the PZ transducers simultaneously to maintain high pressure between the electrodes of the spark gap using constructive interference. The minimum period between PZ pulses is a function of the capacitor charging constant of the PZ transducer and requires detailed analysis.

Arrangement B uses a sequence of PZ transducer pairs. Each transducer is placed 180° apart from its pair. Both PZ transducers in each pair actuate simultaneously to create a region of high pressure between the electrodes via constructive interference. The pairs fire sequentially, maintaining the high-pressure region until the TRV subsides. Spacing and number of PZ transducers provides a particular point of investigation.

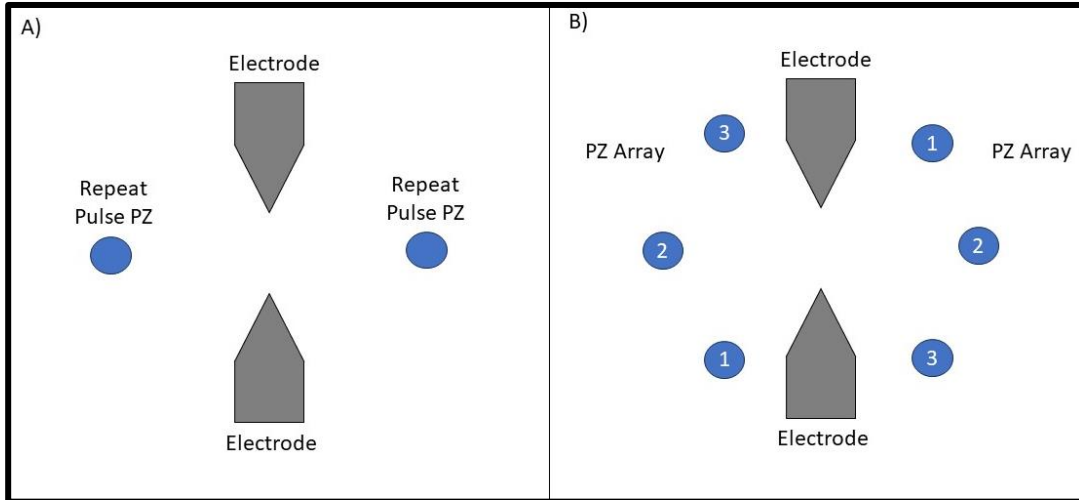


**Figure 36.** Possible PZ arrangements. A) A PZ array that uses two repeatedly pulsing PZ transducers. B) A PZ array that uses sequentially operating PZ transducer pairs.

*Example Scenario of PZ Timing and Current PZ Technology Limitations*

An example scenario helps to clarify the PZ timing challenges. Under the conditions simulated, the TRV subsides within 0.03 seconds. The standing pressure wave must last the entire duration of the TRV. Neglecting the oscillations associated with the PZ pulses, each pulse takes approximately 0.033 milliseconds. Therefore, the breaker control system must actuate the PZ transducers a minimum of 1,100 times. For a single PZ transducer array, this results in a pulse repetition frequency of 33.3 kHz.

Furthermore, the energy required for PZ actuation may be determined using the same firing circuit presented by Thomas, et al. [11]. For each pulse, the energy consumption is equal to the sum of the energy to charge the positive charging capacitor and the negative discharging capacitor. Over 1,100 pulses, the energy required is about 45 kilojoules or 0.02 kilowatt-hours, a minimal amount of energy that could be stored in an ultracapacitor or small battery pack.

The market for high power PZ transducers is relatively small and is generally limited to those used in medical applications. In fact, many high-power PZ transducers are generally custom ordered through companies such as PI or Piezo Technologies. The high-power PZ transducers used in lithotripsy typically operate in the several hertz range. For example, the Richard Wolfe PiezoWave operates at frequencies varying from one to eight hertz [15]. However, Piezo Technologies offers the ability to develop high power transducers over a frequency range of 20 kHz to 20 MHz and size range of 0.5 inches to 8 inches [16].

### *Possible Methods of Breaker Failure*

Any new type of technology required for the safety of electrical systems requires a detailed study of failure analysis. While an exhaustive study must be completed prior to full-scale development and implementation of this new breaker design, this section highlights a four of the most likely failure scenarios. Risk levels of low, medium, and high correspond to the consequences of the failure scenario to people and equipment.

The first scenario is failure of the electrical arc to transfer from the main breaker contacts to the arc chamber. Eventually, the breaker contacts would open far enough that air would sufficiently insulate and extinguish the arc. In this case, the main breaker contacts would endure wear the entire duration of the arc. This is an example of a low-risk failure.

The second scenario is failure of one or more PZ transducers. Failure could be defined as inaccurate timing of actuation, failure to actuate, or failure to produce the expected pressure pulse. All these sub-scenarios may prevent the pulse from being sufficiently strong enough to extinguish the arc. This means that the arc may remain in the spark gap until the TRV subsides below the steady state breakdown voltage of the liquid medium. This is an example of a medium risk failure.

The third scenario is failure of the pressure chamber. Should liquid CO<sub>2</sub> be employed, the steady-state pressure in the chamber would be on the order of hundreds of pounds per square inch. Failure of the vessel at these pressures could result in leaks or sprays that pose a significant risk to personnel. When the pulse is actuated, pressures can reach thousands of pounds per square inch. These pressures not only pose a risk to personnel in the event of leaks, but also risk rapid fracturing of the chamber and possible shrapnel. However, it is important to note that the pressures generated by the pulse are only localized in nature and the wall of the pressure chamber would not be subjected to such high pressures under normal conditions. Because of the personnel risks involved, pressure chamber failure is an example of a high-risk failure.

The final scenario is an electrical short across the arc chamber spark gap. The spark gap in the arc chamber requires a very small distance to allow the gap to be conductive enough to initiate an arc during a fault but insulated enough to prevent current flow during steady state operation. A piece of debris between the electrodes or shock to the arc chamber causing the electrodes to touch could result in severely high electrical currents that bypass the main breaker

contacts, resulting in a fault that can only be stopped by an upstream breaker operating. As such, this is an example of a high-risk failure.

## Chapter 6: Conclusion

This work presented a new mechanical AC breaker that prevents or disrupts electric arc formation across the main breaker contacts by placing a liquid-filled arc chamber in parallel with the main breaker contacts. The two primary operating principles of this breaker concept are the transfer of any electric arc from the main breaker contacts to the arc chamber and the modulation of dielectric properties of the liquid by applying high pressure through shock waves from a piezoelectric transducer array.

MATLAB/Simulink models assessed these operating principles based on physical equations and experimental data collected by Young and Thomas, et al [6], [11]. Based on assumptions that must be verified through laboratory experimentation, the MATLAB/Simulink models presented show promise and demonstrate the plausibility of this new breaker concept.

Successful development and implementation of this breaker design would reduce reliance on gas insulating breakers such as SF<sub>6</sub> breakers in AC systems. Additionally, the parallel arc chamber itself may serve as an alternative to traditional arc chute designs in T&D AC breakers. Large and bulky, arc chutes extinguish the arc by dividing and cooling it. The parallel placement of the arcing chamber moves the arc extinguishment capability outside the breaker. This may allow a utility company to use only a disconnect switch, relying on the arc chamber to break fault current. However, the advantage in using a smaller, cheaper disconnect may come as a tradeoff to a large and bulky arc chamber placed next to it.

The implications of the modulation of the dielectric properties of the liquid via pressure are far reaching. Throughout this paper, the applications and designs associated with this breaker were specific to AC systems. This breaker type finds value in direct current (DC) arc extinguishment systems. Briefly, DC systems have a unique disadvantage in that there is not a naturally occurring current zero-crossing. This means that a DC breaker must break current and dissipate its associated inductive energy. Modulation of the dielectric properties in a DC breaker may extinguish the arc temporarily while another system consumes or stores the energy associated with the inductive nature of the DC current chop.

## REFERENCES

- [1] U.S. Environmental Protection Agency, U.S. Environmental Protection Agency, 14 April 2023. [Online]. Available: [https://www.epa.gov/eps-partnership/sulfur-hexafluoride-sf6-basics#:~:text=Greenhouse%20Gas,-Sulfur%20hexafluoride%20\(SF&text=Over%20a%20100%2Dyear%20period,atmospheric%20lifetime%20of%203%2C200%20years](https://www.epa.gov/eps-partnership/sulfur-hexafluoride-sf6-basics#:~:text=Greenhouse%20Gas,-Sulfur%20hexafluoride%20(SF&text=Over%20a%20100%2Dyear%20period,atmospheric%20lifetime%20of%203%2C200%20years.). [Accessed 7 December 2023].
- [2] L. Yuan, L. Sun and H. Wu, "Simulation of Fault Arc Using Conventional Arc Models," January 2013. [Online]. Available: [https://www.scirp.org/pdf/EPE\\_2013111115514404.pdf](https://www.scirp.org/pdf/EPE_2013111115514404.pdf). [Accessed 10 May 2023].
- [3] F. Yang, Z. Tang, Y. Shen, L. Su and Z. Yang, "Parameter Determination Method of Cassie-Mayr Hybrid Arc Model Based on Magnetohydrodynamics Plasma Theory," 8 April 2022. [Online]. Available: <https://www.frontiersin.org/articles/10.3389/fenrg.2022.808289/full>. [Accessed 29 August 2023].
- [4] F. M. Locke, "Electric-Arc Extinguisher". United States of America Patent 1127043, 2 February 1915.
- [5] E. A. Alegria, "Modeling Transient Recover Voltage of a 34.5 kV Expulsion Fuse," January 1991. [Online]. Available: <https://www.proquest.com/docview/2700338924?pq-origsite=gscholar&fromopenview=true>. [Accessed 27 February 2023].
- [6] D. R. Young, "Journal of Applied Physics," 26 September 1949. [Online]. Available: <https://doi.org/10.1063/1.1699638>. [Accessed 27 March 2023].
- [7] P. Wedin, "Electrical Breakdown in Dielectric Liquids - A Short Overview," 2014. [Online]. Available: <https://doi.org/10.1109/MEI.2014.6943430>. [Accessed 27 March 2023].
- [8] O. Lesaint and P. Gournay, "On the gaseous nature of positive filamentary streamers in hydrocarbon liquids. I: influence of the hydrostatic pressure on the propagation," 14 July 1994. [Online]. Available: <https://doi.org/10.1088/0022-3727/27/10/019>. [Accessed 27 March 2023].
- [9] R. Cleveland and J. McAteer, "Physics of Shock-Wave Lithotripsy. In Smith's Textbook of Endourology (eds A.D. Smith, G.H. Badlani, G.M. Preminger and L.R. Kavoussi),"

2012. [Online]. Available: <https://doi.org/10.1002/9781444345148.ch49>. [Accessed 17 April 2023].
- [10] D. Cathignol. United States Patent 7264597 B2, 2007.
- [11] G. P. Thomas, J.-Y. Chapelon, A. Birer, C. Inserra and C. Lafon, "Confocal lens focused piezoelectric lithotripter," 7 December 2019. [Online]. Available: <https://doi.org/10.1016/j.ultras.2020.106066>. [Accessed 9 March 2023].
- [12] E. W. Lemmon, I. H. Bell, M. L. Huber and M. O. McLinden, "Thermophysical Properties of Fluid Systems," 2023. [Online]. Available: <https://doi.org/10.18434/T4D303>. [Accessed 27 June 2023].
- [13] R. Cheung, "Matlab script for digitizing a published graph," 2023. [Online]. Available: [https://www.mathworks.com/matlabcentral/fileexchange/36904-matlab-script-for-digitizing-a-published-graph?s\\_tid=FX\\_rc1\\_behav](https://www.mathworks.com/matlabcentral/fileexchange/36904-matlab-script-for-digitizing-a-published-graph?s_tid=FX_rc1_behav). [Accessed 2 August 2023].
- [14] A. Hopf, J. A. Britton, M. Rossner and F. Berger, "Dielectric strength of SF6 substitutes, alternative insulation gases and PFC-gas-mixtures," June 2017. [Online]. Available: <https://doi.org/10.1109/EIC.2017.8004635>. [Accessed 15 November 2023].
- [15] Richard Wolf, "PiezoWave," Richard Wolfe, GmbH, 2023. [Online]. Available: [https://www.richard-wolf.com/mam/data/Typo3/Sonstige\\_Downloads/Sto%C3%9Fwelle/ESWT\\_607\\_PiezoWave\\_GB\\_V09.pdf](https://www.richard-wolf.com/mam/data/Typo3/Sonstige_Downloads/Sto%C3%9Fwelle/ESWT_607_PiezoWave_GB_V09.pdf). [Accessed 7 December 2023].
- [16] Piezo Technologies, "High Power Transducers," Piezo Technologies, 2023. [Online]. Available: <https://piezotechnologies.com/high-power-transducers/>. [Accessed 7 December 2023].

## APPENDIX

The following section describes the calculations that describe the TRV experienced by the test system during simulation. The TRV derived serves as the minimum breakdown voltage that the PZ pulse system must achieve.

The system voltage (V) base, apparent power (VA) base, percent impedance (%Z), and  $X/R$  ratio define the line resistance and impedance by the following equations.

$$(10) \quad Z_{base} = \frac{V_{base}^2}{VA_{base}}$$

$$(11) \quad Z_{actual} = \frac{\%Z}{100} Z_{base}$$

$$(12) \quad R_{line}^2 + X_{line}^2 = Z^2$$

The TRV simulation begins with calculating voltages and currents associated with the pre-fault system. The purpose of these calculations is to determine the initial conditions for fault insertion calculations. Figure 37 shows the test system in its normal operating state prior to the fault insertion.

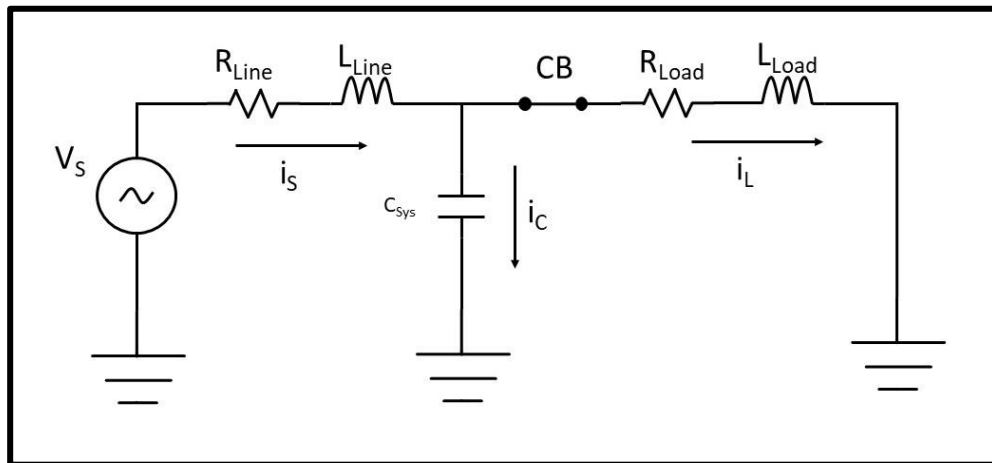


**Figure 37.** Simulated T&D system prior to fault insertion.

By Kirchoff's Voltage Law (KVL) and Kirchoff's Current Law (KCL), Equations 13-15 describe the pre-fault system. Given the initial conditions shown in Equations 16-19, the Simulink model calculates and maintains steady state voltages and currents associated with the

system prior to the fault insertion. These calculations continue until the predetermined fault insertion time,  $t_{\text{fault}}$ .

$$(13) \quad V_S - R_{\text{Line}} i_S - L_{\text{Line}} \frac{di_S}{dt} - \frac{1}{C_{\text{Sys}}} \int i_C dt = 0$$

$$(14) \quad V_S - R_{\text{Line}} i_S - L_{\text{Line}} \frac{di_S}{dt} - R_{\text{Load}} i_L - L_{\text{Load}} \frac{di_L}{dt}$$

$$(15) \quad i_S - i_C - i_L = 0$$

$$(16) \quad i_S(0) = 0$$

$$(17) \quad i_C(0) = 0$$

$$(18) \quad i_L(0) = 0$$

$$(19) \quad V_C(0) = 0$$

$$(20) \quad \frac{dV_C}{dt}(0) = 0$$

The TRV simulation next proceeds to voltage and current calculations associated with the fault insertion. At the time of the fault insertion, the fault fully short circuits the load, reducing the load impedance to zero.

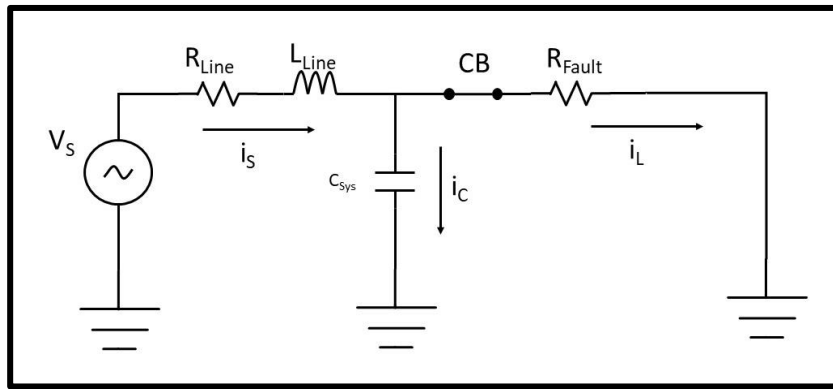


**Figure 38.** Simulated T&D system at the time of the fault insertion.

By KVL and KCL, Equations 21-23 describe the system at the time of the fault. Given the initial conditions in Equations 24-28 calculated previously, the Simulink model calculates the voltages and currents associated with the faulted system. These voltages and currents are used to determine the initial conditions for the system recovery when the main circuit breaker opens. These calculations occur until the time at which the main circuit breaker opens.

$$(21) \quad V_S - R_{Line}i_S - L_{Line} \frac{di_S}{dt} - \frac{1}{C_{Sys}} \int i_C dt = 0$$

$$(22) \quad V_S - R_{Line}i_S - L_{Line} \frac{di_S}{dt} - R_{Fault}i_L = 0$$

$$(23) \quad i_S - i_C - i_L = 0$$

$$(24) \quad i_S(0) = i_S(t_{fault})$$

$$(25) \quad i_C(0) = i_C(t_{fault})$$

$$(26) \quad i_L(0) = i_L(t_{fault})$$

$$(27) \quad V_C(0) = V_C(t_{fault})$$

$$(28) \quad \frac{dV_C}{dt}(0) = \frac{dV_C}{dt}(t_{fault})$$

The TRV simulation next proceeds to voltage and current calculations associated with the fault recovery. The TRV associated with the fault recovery occurs when the main circuit breaker begins to open. A slight delay occurs before the breaker begins to open because the protection system must first detect the fault. Equation 29 describes the time at which the breaker opens when accounting for this delay. Figure 39 shows the system at the time the breaker opens.

$$(29) \quad t_{open} = t_{fault} + t_{delay}$$

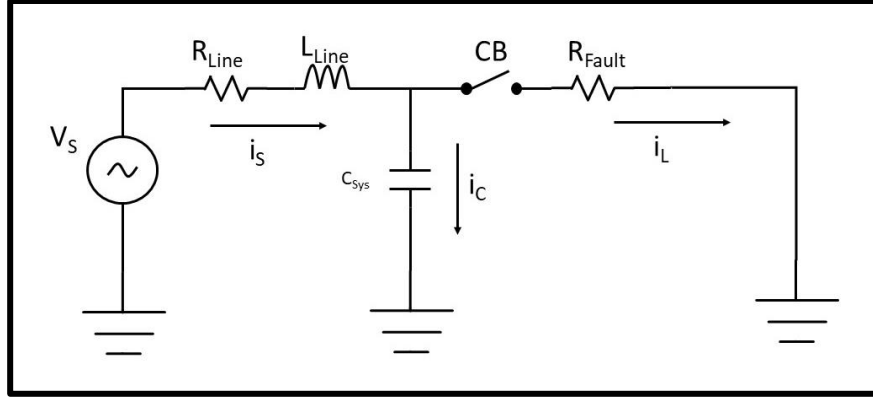


**Figure 39.** Simulated T&D system at the time of fault clearing.

By KVL and KCL, Equations 30 and 31 describe the system at the time the breaker opens. Given the initial conditions in Equations 32-35 calculated previously, the Simulink model calculates the voltages and currents associated with the recovering system. These voltages and currents are used to determine the initial conditions for the system recovery when the main circuit breaker opens. Given Equation 36, the Simulink model calculates the voltage across the capacitor which is equivalent to the TRV.

$$(30) \quad V_s - R_{Line}i_s - L_{Line} \frac{di_s}{dt} - \frac{1}{C_{Sys}} \int i_c dt = 0$$

$$(31) \quad i_s - i_c = 0$$

$$(32) \quad i_s(0) = i_s(t_{open})$$

$$(33) \quad i_c(0) = i_c(t_{open})$$

$$(34) \quad V_c(0) = V_c(t_{open})$$

$$(35) \quad \frac{dV_c}{dt}(0) = \frac{dV_c}{dt}(t_{open})$$

$$(36) \quad TRV = V_c = \frac{1}{C_{Sys}} \int i_c dt$$